BNL-114201-2017-JA

Ceria-based model catalysts: Fundamental studies on the importance of the metal-ceria interface in CO oxidation, the water-gas shift, CO2 hydrogenation, and methane and alcohol reforming

J. A. Rodriguez

Submitted to Chemical Society Reviews

August 2017

Chemistry Department

Brookhaven National Laboratory

U.S. Department of Energy
USDOE Office of Science (SC),
Basic Energy Sciences (BES) (SC-22)

DISCLAIMER

Ceria-based model catalysts: Fundamental studies on the importance of the metal-ceria interface in CO oxidation, the water-gas shift, CO_2 hydrogenation, and methane and alcohol reforming

José A. Rodriguez,[a,b]* David C. Grinter,[a] Zongyuan Liu,[b] Robert M. Palomino[a] and Sanjaya D. Senanayake[a]

[a] Chemistry Department, Brookhaven National Laboratory, Upton, New 11973.
[b] Department of Chemistry, State University of New York (SUNY), Stony Brook, NY 11749.

*Corresponding author. E-mail : rodrigez@bnl.gov

Abstract

Model metal/ceria and ceria/metal catalysts have shown to be excellent systems for studying fundamental phenomena linked to the operation of technical catalysts. In the last fifteen years, many combinations of well-defined systems involving different kinds of metals and ceria have been prepared and characterized using the modern techniques of surface science. So far most of the catalytic studies have been centered in a few reactions: CO oxidation, the hydrogenation of CO_2, and the production of hydrogen through the water-gas shift reaction and the reforming of methane or alcohols. Using model catalysts it has been possible to examine in detail possible correlations between the structural, electronic and catalytic properties of ceria-metal interfaces. *In-situ* techniques (X-ray photoelectron spectroscopy, X-ray absorption spectroscopy, Infrared spectroscopy, Scanning tunneling microscopy) have been combined to study morphological changes under reaction conditions and investigate the evolution of active phases involved in the cleavage of C-O, C-H and C-C bonds. Several studies with model ceria catalysts have shown the importance of strong metal-support interactions. In general, a substantial body of knowledge has been acquired and concepts have been developed for a more rational approach to the design of novel technical catalysts containing ceria.

1. Introduction

Cerium oxide (CeO_2) is widely used in many areas of heterogeneous catalysis.[1] It has received a lot of attention due to its ability to switch between Ce^{4+} and Ce^{3+} oxidation states.[2] It adopts a fluorite-type crystal structure in which each Ce cation is surrounded by eight oxygen atoms. The coordination number of the oxygen atoms is four. The crystal structure can be seen as combination of CeO_8 cubes or OCe_4 tetrahedra. In its various micro- and nanoparticle formulations, ceria is fast gaining a reputation as a 'super-material' with applications in technical areas beyond heterogeneous catalysis, such as the fabrication of optical devices, fuel additives, mechanical polishing, and solid oxide fuel cells.[3]

Catalysts which contain ceria may come on the three configurations show in Scheme I: metal/oxide, oxide/metal and {oxide+metal}/oxide. The metal/oxide configuration is by far the most common in industrial applications.[2,4] It has the disadvantage that bulk ceria is a stable oxide support which have a limited chemical activity. To model this configuration people have used single crystals[5] or well-defined oxide films grown on top of a metal substrate[6,7,8,9] or on another oxide.[10,11] The inverse oxide/metal configuration is less common in technical applications[12,13,14] but it is quite useful for fundamental studies in catalysis.[15,16,17,18,19] It can lead to very strong metal-oxide interactions.[20,21] An inverse oxide/metal configuration is frequently generated by vapor depositing ceria nanoparticles on a well-defined single crystal of a metal.[15-19, 22] Finally, a composite {oxide+metal}/oxide configuration takes advantage of the intrinsic properties of mixed-metal oxides[23,24,25,26,27,28] and can be quite powerful since it combines the properties of nanoceria and metal nanoparticles.[29,] In many cases, it leads to high catalytic activity.[30,31] Model catalysts for this configuration can be generated by depositing nanoparticles of ceria and a metal on top of a single crystal surface of a second oxide.[32] Model catalysts with the configurations shown in Scheme I have been extensively used to study process associated with the removal of CO as a pollutant,[8,16,18] the conversion of CO_2 into valuable chemicals,[21,33] and the production of hydrogen through the water-gas shift and the reforming of methane and alcohols.[5,28,34,35]

This article is organized as follows. First, we will discuss several approaches used for the preparation and characterization of different types of ceria model catalysts. Then, we will discuss how these systems have been used to study the chemistry associated with several catalytic processes: Oxidation of CO, the water-gas shift reaction, CO_2 hydrogenation to methanol, the activation and conversion of methane, and the reforming of alcohols. The ceria model catalysts have provided a fundamental understanding of chemical phenomena relevant for these catalytic processes, pointing also to new ways to improve the performance of industrial or technical catalysts.

2. Preparation and characterization of ceria-model catalysts

The most stable surface of bulk ceria involves the (111) plane of the fluorite structure. To study the reactivity of this surface researchers have used single crystals[5] or films.[6-11] Over the last couple of decades, a wide range of single crystal metal substrates have been employed to support well defined ceria films and nanostructures, including Ru(0001),[34] Pt(111), [36] Rh(111), [37] Ni(111),[6] Au(111),[17] Cu(111),[33] Re(0001), [38] and Pd(111). [39] Accompanying this variety in support, there has been an assortment of preparation recipes for both thin ceria films and nanostructures.[40] In Scheme II, we summarize some of the most popular methods.

The most commonly used procedure, pioneered by Mullins et al,[6,40] is the so-called reactive deposition, where cerium is evaporated via physical vapor deposition onto a heated substrate in a background pressure of oxygen, followed by an annealing stage which orders the ceria. By varying the oxygen partial pressure during the deposition and annealing stages, it is possible to control the stoichiometry of the films.[40] A variation on this was employed by the Freund group in an attempt to prepare flatter ceria layers more suitable for high resolution scanning tunneling microscopy (STM) studies, and can be thought of as a kinetically limited growth process.[41] In this method, the first few layers of ceria are deposited at cryogenic temperatures to facilitate the formation of the first interfacial layer between the oxide and the support (which often display a lattice mismatch of up to 40%). Further layers

are deposited as the temperature is increased, with a final high temperature oxidation step to order the film and increase the degree of crystallinity.[41] A third method, pioneered by Schierbaum et al., prepares ceria via the oxidation of Ce-M surface alloys.[42] A high temperature annealing step in ultra-high vacuum (UHV) immediately after cerium deposition yields well-ordered surface alloy phases, which are subsequently oxidized to form CeO_2(111); this approach has been demonstrated to form particularly well-ordered inverse ceria islands on Pt(111).[22,43] Another alternative approach, differing from the physical vapor-deposition (PVD) growth methods described above, is to use pulsed laser deposition from a cerium target. This has been employed for ceria growth on $SrTiO_3$(100), which yields CeO_2(100)-oriented films.[44]

Supported ceria films and nanostructures display a rich variety of morphologies and chemistry, and are generally split into two systems: i) complete coverage films, and ii) inverse model catalysts (partial surface coverage). Given the limited thickness of the ceria, (<5 nm in most cases) it is generally possible to apply standard surface science techniques without encountering undesirable charging problems. The primary tool for probing the structure in real space is STM; typical images of complete coverage CeO_2(111) films on Ru(0001) are shown in Figure 1.[45]

During the preparation of the ceria films shown in Figure 1, the oxygen pressure was varied to give different stoichiometries. In the fully oxidized film (Figure 1A) the (111) terraces are clearly visible with very straight step edges (inset shows the atomically resolved lattice); as the film becomes progressively more oxygen deficient, (Figure 1B, 1C) the terraces are observed to roughen as the density of oxygen vacancies increases and become more rounded. A unique strength of the STM technique is the ability to probe the atomic structure of surfaces, down to the level of individual defects and adsorbates. Figure 2 shows one such image, obtained on the surface of a CeO_2(111)/Pt(111) system.[43]

The image in Figure 2 was obtained at a sample bias of -3 V, and therefore the bright lattice corresponds to tunneling out of filled states at the surface, mostly due to the oxygen atoms. It is possible to identify a range of surface features including surface oxygen

vacancies, hydroxide species, and water molecules. Following the behavior of CeO_2(111) surfaces under reaction conditions will be key to future understanding of the mechanistic role and importance of individual defects. Ambient pressure STM (AP-STM, generally up to pressures of a few Torr) is helping to achieve this goal; recent in situ studies of the reduction of CeO_2/Cu(111) by H_2 have highlighted how the inverse ceria nanostructures change during the reaction.[33] In addition to extensive STM studies, the CeO_2/Pt(111) system has also been probed using high-resolution scanning transmission electron microscopy (STEM) and electron energy loss spectroscopy (EELS), providing new insights into the variation of cerium oxidation state at the metal-oxide interface.[46]

Inverse model ceria catalysts are powerful motifs for studying the interfaces between the ceria and the supporting metal,[47] and display a diverse range of structures, as shown in the comparison in Figure 3, where CeO_2(111) has been prepared on Au, Pt, Re, Rh, Ru, and Cu. The variation in island shape and morphology is clear from the STM and low-energy electron microscopy (LEEM) images in Figure 3. The diffraction patterns also indicate the wealth of differences between the systems, partially a result of the discrepancy in lattice parameter between the ceria (3.83 Å) and the metal supports (2.88-2.55 Å) which leads to varying strain at the metal-oxide interface. Another aspect to consider is the reactivity of the support – under common ceria preparation conditions, Cu(111) forms a surface oxide (Cu_2O),[33] and Rh(111)[37] and Ru(0001)[48] gain a chemisorbed O-(2 x 2) layer. Some of the ceria films also display rotational phases (Re, Ru) rather than a pure epitaxial structure (Au, Pt, Rh, Cu); this is usually a result of the precise preparation procedure and especially the temperature control.[48,49]

An example of the variation in surface structure when employing different growth conditions is demonstrated in Figure 4 for the CeO_2/Cu(111) system. By varying the oxygen chemical potential during the growth, the experimenters were able to tune the surface termination of the ceria; at low O_2 potential the (111) surface is favored whereas at high O_2 potential the (100) surface prevails.[50]

Although STM is the most common characterization tool, LEEM and X-ray photoemission electron microscopy (XPEEM) have proved to be powerful probes of the structure and reactivity of CeO_2 on Pt(111),[36] Rh(111),[37,51] Ru(0001),[48,52,53,54] Cu(111)[50,55] and Re(0001).[38] A key strength of these techniques is their ability to probe dynamic processes in real time under varying sample conditions, (100-2000 K, UHV-10^{-5} Torr) which proves especially useful for studying the high temperature growth procedures of the ceria films and nanostructures.[48-50] Figure 5 demonstrates the power of the LEEM/XPEEM instrument for the characterization of inverse CeO_2(111) islands on Rh(111) using a range of measurement modes. Figure 5A displays the low-energy electron diffraction (LEED) pattern, consisting of the (1 × 1) reflexes from the Rh substrate, a (2 × 2) oxygen overlayer, and the (1.4 × 1.4) spots from the ceria. A bright-field (0,0) LEEM image is shown in Figure 5B; the substrate step edges are clear nucleation sites of the ceria islands, which have quasi-hexagonal shapes and lateral dimensions of tens to hundreds of nanometres. A composite dark-field LEEM image ((1,0) and (0,1)) is shown in Figure 5F, confirming that the islands are the main contribution to the ceria diffraction pattern. An XPEEM image acquired in secondary (PEY) mode at the Ce M_4 edge (Figure 5C) confirms the assignment of the islands as composed of ceria, with the corresponding XAS spectrum (Figure 5G) indicating that the islands are stoichiometric CeO_2 (Ce^{4+}). XPEEM imaging acquired in energy-filtered (XPS) mode at the O 1s maximum (Figure 5D and 5H) shows oxygen is present all over the surface, as expected from the (2 x 2) LEED pattern in Figure 5A, but with a greater amount in the ceria islands. Acquiring an XPEEM image at the Rh $3d_{5/2}$ maximum (Figure 5E) demonstrates the attenuation by the ceria of the photoelectrons emitted from the substrate. Comparing Rh 3d XPS spectra (Figure 5I) obtained from the islands (green line) and the substrate (red line) permits an accurate measurement of the thickness of the ceria, in this case ~0.8 nm (2-3 CeO_2 trilayers).

Complete coverage ceria films have been used as a support for metal nanoparticles in an attempt to study the interface between the oxide and the constrained metal, which often displays interesting chemical properties. Examples of metals/ceria investigated so far

include Au,[56] Ag,[57] Pt,[45] Pd,[58] Cu,[59] Ni,[6] Rh,[60] Sn,[61] W,[62] Ga,[63] and Co.[64] These are generally deposited in UHV by PVD onto the surface of the ceria films. STM is generally used to characterize their morphology, a few examples of which are shown in Figure 6.

The gold-ceria system has been intensely studied for many years. Figure 6A shows how STM was used to probe the defect structure of a ceria film (dark spots are oxygen vacancies) before and after the deposition of Au single atoms at 300 K.[56] Despite a thermodynamic preference for binding to vacancies, the adsorbed gold atoms encounter significant diffusion barriers and bind to standard surface sites. Larger metal particles display interesting effects depending on the degree of interaction with the CeO_2(111) surface. Figure 6B shows the adsorption of bimetallic Au+Pt particles after annealing to 800 K; the particles exhibit hexagonal shapes and are mostly located at the step edges of the ceria.[65] The ceria support also influences the nanoparticle morphology, as seen for the Ni/CeO_2(111) system in Figure 6C. The fully oxidized CeO_2 results in large particles at the step edges, whereas the reduced CeO_{2-x} supports a higher density of smaller particles distributed across the terraces as well.[66] Table 1 presents a summary of the various metals used as substrates for the growth of ceria films (CeO_x/M), and those investigated as supported metal nanoparticles. (M/CeO_2(111))

CeO_x/M	**M/CeO_2(111)**
-	Co[64]
Ni(111)[6]	Ni[34]
Cu(111)[33]	Cu[59]
-	Ga[63]
Ru(0001)[6]	-
Rh(111)[37]	Rh[60]
Pd(111)[39]	Pd[58]
-	Ag[57]
-	Sn[61]
-	W[62]
Re(0001)[38]	-
Pt(111)[43]	Pt[45]
Au(111)[17]	Au[56]

Table 1. A comparison of the metals used as substrates for CeO_2(111) films and those deposited as supported nanoparticles.

In addition to the ceria-metal interfaces summarized in Table 1, there has been a great deal of work studying the interface of ceria with other oxides, in particular titania. One route to this has been by depositing ceria onto a TiO_2 surface, i.e. $CeO_x/TiO_2(110)$, which forms an effective catalyst for water-gas-shift and CO_2 hydrogenation reactions when combined with metal nanoparticles such as Pt, Au, or Cu.[30,32,33,67,68] A second method to generate a mixed oxide with intimate connections between the phases has been the co-deposition of metals during the formation of the ceria film, as illustrated by Zhou et al. for the $TiO_x/CeO_x/Ru(0001)$ system.[69,70]

3. CO oxidation

Since the classic work of Langmuir in 1922, the oxidation of CO over Platinum group metals has been the subject of a very large number of experimental and theoretical studies.[71] In the last twenty years, CO oxidation has attracted renewed attention due to its technological importance in the area of pollution control and fuel cells. Recent studies with powder catalysts point to strong electronic interactions between Pt and ceria that can improve the performance of the catalyst.[72] These strong interactions have been observed in the case of $Pt/CeO_2(111)$ and $CeO_x/Pt(111)$ model catalysts.[15,22,73] These interactions affect the reactivity of Pt towards CO modifying its ability to dissociate the molecule through a disproportionation reaction ($2CO \rightarrow C + CO_2$). At the same time, the Pt-CeO_2 interactions enhance the sticking coefficient of O_2.[18]

Figure 7 displays data for the oxidation of CO on Pt(111) and over $CeO_x/Pt(111)$ surfaces pre-covered with 0.3 and 0.7 ML of the oxide.[18] In the case of {CO + O}/Pt(111), on the macroscopic scale, two stable steady states have been observed: a state of *low-reactivity* with a surface mostly covered by CO and a state of *high-reactivity* with a predominantly oxygen-covered surface. A modification of the reaction conditions can lead to kinetic transitions between these two states and a hysteric loop has been observed.[18] In Figure 7c, the red curve shows kinetic data for CO oxidation on plain Pt(111). It starts with a low pressure of CO within the steady state of high reactivity which loses its stability upon

approaching the transition point τ_A. For the reverse scan the steady state of low reactivity becomes unstable at τ_B. The STM images at the top of Figure 7 give the dispersion of ceria particles on the platinum substrate. On these surfaces the oxidation of CO occurs faster than on plain Pt(111), Figure 7c,d. This is mainly due to a ceria-enhancement in the sticking coefficient of O_2.[18] The co-deposition of Pt and ceria nanoparticles on TiO_2(110) produces catalysts with an extreme activity for CO oxidation, much more active than Pt/CeO_2 or Pt/TiO_2.[30,32] On the titania substrate, a very active Pt-ceria interface is formed. [30,32]

Precious metals used as catalysts for CO oxidation can undergo rapid deactivation due to the presence of small amounts of impurities.[71] Noble metal-free catalysts have been explored lately. Especially, copper and copper-based catalysts have been the focus of much attention because of their superior catalytic activity towards the oxidation of CO in regular and hydrogen-rich (PROX) streams.[12,74,75] A Cu(111) surface displays a low activity for the oxidation of carbon monoxide, Figure 8. The addition of ceria nanoparticles to Cu(111) produces a substantial enhancement in the catalytic activity of the system, Figure 8.[76] The morphology of the surface changes during cycles of reduction and oxidation. The results of theoretical calculations indicate that the Ce^{3+} sites in a CeO_x/Cu(111) system shown adsorb O_2, dissociate the molecule, and release atomic O for reaction with CO in an efficient way.[76] The inverse CeO_x/Cu(111) catalysts display activities for the CO oxidation process that are comparable with or larger than those reported for surfaces of expensive noble metals such as Rh(111), Pd(110) and Pt(100).[76] The key to this activity is the existence of Ce^{3+} sites in the oxide-metal interface which bind O atoms weaker than the Ce^{3+} sites of bulk ceria.[76]

4. Water-gas shift reaction

Currently, the primary source of hydrogen for the chemical and petrochemical industries comes from the steam reforming of hydrocarbons: $C_nH_m + nH_2O \rightarrow nCO + (n-m/2)H_2$. The reformed fuel usually contains 1-10% of CO, an impurity that can be a serious problem for chemical processes which use H_2 as a feedstock and for the operation of fuel

cells. CO oxidation and the water-gas shift reaction (WGS, $CO + H_2O \rightarrow H_2 + CO_2$) are critical processes for providing clean hydrogen.[4] Ceria is an interesting support in a new generation of WGS catalysts[4] due to its ability to react and dissociate water on O vacancies or Ce^{3+} sites. The WGS reaction has been studied on $Au/CeO_2(111)$, $Cu/CeO_2(111)$, $Ni/CeO_2(111)$ and $Pt/CeO_2(111)$ surfaces.[5,73,77] Figure 9 compares the activity of these systems under similar reaction conditions (20 Torr of CO and 10 Torr of H_2O at 625 K). The Pt-based catalyst is clearly the best in terms of activity and low loading of the admetal. The $Au/CeO_2(111)$ and $Cu/CeO_2(111)$ catalysts display a better performance than $Pt/CeO_2(111)$ only at high loadings of the admetal (> 0.3 ML) when the catalytic activity drops likely due to the fact that most of the Pt atoms are no longer in contact with the ceria surface.[73]

A study of the WGS on Pt(111) indicates that there can be problems to perform the reaction on extended surfaces of platinum.[78] The turnover frequency of Pt(111) is initially five times greater than that observed on Cu(111), a typical benchmark for the WGS reaction,[79,80,81] but Pt(111) undergoes deactivation due to the deposition of carbon by the Boudouard reaction: $2CO(surf) \rightarrow C(surf) + CO_2(gas)$.[78] Metal↔support interactions prevent this phenomenon and enhance the forward WGS on $Pt/CeO_2(111)$.[73] The reported catalytic activity in Figure 9 correlates with the magnitude of the electronic perturbations seen in UPS measurements, Figure 10. The $Pt/CeO_2(111)$ catalysts with the highest activity (Θ_{Pt} < 0.3 ML) displayed a lower density of Pt 5d states near the Fermi level (Figure 10), while the catalysts with lower activity (Θ_{Pt} > 0.8 ML) exhibited a density of Pt 5d states near the Fermi level which was not much different from that of bulk metallic Pt(111).[73] The results of density-functional calculations point to a facile dissociation of water on small Pt clusters electronically perturbed by interactions with ceria. In contrast, the barrier for dissociation of the molecule on Pt(111) is quite high.[73,78] Assuming that all the Pt atoms deposited on $CeO_2(111)$ participate in the reaction, one can estimate turnover frequencies of 12.4 (Θ_{Pt}= 0.15 ML) and 11.5 (Θ_{Pt}= 0.25 ML) molecules Pt_{site}^{-1} s^{-1} for the highly active catalysts in Figure 9.[73] These values represent a lower limit for the turnover frequencies, because only

the surface atoms of the clusters or Pt particles should behave as active sites. In any case, the estimated turnover frequencies for the $Pt/CeO_2(111)$ systems are *much larger* than the value of 0.53 molecules Pt_{site}^{-1} s^{-1} reported for the Pt(111) surface.[78] Strong metal-support interactions have also been detected for the $Ni/CeO_2(111)$ system.[77] The interactions suppress the ability of Ni to perform the CO methanation reaction and favor the WGS process.[77]

Inverse CeO_x/Au(111) and CeO_x/Cu(111) catalysts have been quite useful to study the WGS reaction.[17,81] Au(111) does not catalyse the WGS process by itself but upon addition of ceria becomes a very good catalyst, Figure 11.[17] A very large enhancement of catalytic activity is also seen when going from Cu(111) to CeO_x/Cu(111).[81] The formation of a ceria-copper interface is essential opening a reaction path that has low adsorption energies and low energy barriers for the formation of key intermediates, Figure 11c,d.[82] The ceria nanoparticles help with the dissociation of water and CO adsorbs on Cu sites. At the metal-oxide interface OH and CO react to yield a HOCO intermediate and then an adsorbed $CO_2^{\delta-}$ species that has been detected by near ambient-pressure X-ray photoelectron spectroscopy and infrared spectroscopy.[82] The formation of the HOCO intermediate does not take place on plain Cu(111) where the WGS goes through a redox mechanism instead of an associative mechanism.[79,81,82]

The results in Figures 9 and 11 point to a high activity in the WGS when one has small nanoparticles of the metal or oxide. On the basis of this information, systems of the type $M/CeO_x/TiO_2(110)$ (M= Au, Cu, Pt) were investigated and displayed a superior performance.[30,32,67] In Figure 12, the presence of ceria on the titania surface always leads to an increase in the catalytic activity with respect to plain titania. At small coverages, the ceria grows on the titania forming wire-like structures that are nucleation sites for Cu, Au and Pt.[30,32] The growth mode of ceria changes at medium or large coverages but the oxide structures are still preferred points for the nucleation of metals.[67] On these ceria-metal interfaces the dissociation of water is almost spontaneous[83] and the metal and oxide work in

a synergistic way to create a pool of OH groups which can react with CO.[84] The model $Au/CeO_x/TiO_2(110)$ and $Pt/CeOx/TiO_2(110)$ catalysts have been scaled up to powder $Au/CeO_x/TiO_2$ and $Pt/CeO_x/TiO_2$ catalysts displaying very good activity and stability.[85,86,87]

5. CO_2 hydrogenation to methanol

There is a new interest in the study of the hydrogenation of CO_2 to methanol and higher alcohols ($xCO_2 + yH_2 \rightarrow C_xH_3OH + xH_2O$).[88] The process is interesting because it transform a major atmospheric pollutant into a chemical that can be used as a fuel or the starting point for the preparation of other chemicals and commodity goods. Today this reaction is predominantly associated with supported Cu based catalysts with a $Cu/ZnO/Al_2O_3$ formulation.[14] Cu on its own is a poor catalyst for the $CO_2 \rightarrow CH_3OH$ conversion and has a low propensity to do several key steps that lead to CO_2 activation. An enhancement in the catalytic activity of Cu is frequently observed after dispersing this metal on ZnO or other oxide substrate.[14] Studies have been carried out investigating the transformation of CO_2 into methanol on $CeO_x/Cu(111)$ and $Cu/CeO_2(111)$ catalysts.[21]

Figure 13 shows the rate of methanol production from CO_2 hydrogenation on Cu(111) and on $CeO_x/Cu(111)$ catalysts with several coverages of ceria.[21] In Figure 13A, there is a clear enhancement in methanol production upon the generation of the inverse oxide/metal catalysts. In $CeO_x/Cu(111)$, the highest catalytic activity was found when the Cu(111) surface was 30-40% covered by ceria. No catalytic activity was detected after completely covering the copper substrate, indicating that the $CO_2 \rightarrow CH_3OH$ transformation occurred at the Cu-CeO_x interface. At ceria coverages below 40%, the Ce cations were mostly in a +3 oxidation state that is directly involved in the binding and activation of CO_2.[33] In the Arrhenius plots in Figure 13B, the apparent activation energy for CH_3OH production drops from a value of 25 kcal/mol on Cu(111) to 16 kcal/mol on ZnO/Cu(111) and to 13 kcal/mol on $CeO_x/Cu(111)$.[21] For the temperature range investigated (500-600 K), $CeO_x/Cu(111)$ was always the catalyst with the best performance.[21,33]

The surface chemistry of CeO_x/Cu(111) under reaction conditions was examined using a combination of AP-XPS and ambient-pressure infrared reflection absorption spectroscopy (AP-IRRAS).[21] Figure 14 shows O 1s and C 1s XPS spectra of a fresh CeO_2/CuO_x/Cu(111) surface with ~ 0.2 ML of CeO_x (a), under 30mTorr of CO_2 at 300 K (b), with an addition of 270 mTorr of H_2 (c), and subsequent heating to 400 (d) and 500 K (e) under those conditions. In the O 1s region (left) the primary peak at 530 eV corresponds to the oxygen from CeO_x with a small contribution from the CuO_x/Cu(111) substrate in the as prepared surface (a). In addition, this surface exhibits a small concentration of OH species (531.5 eV). In the C 1s region (right) no peaks are visible except for a small contribution from surface C at 284 eV, likely produced by the decomposition of background gases. With the addition of 30mTorr of CO_2 at 300 K (b), peaks centered at 531.9 eV (O 1s) and 289.3 eV (C 1s) are now visible that can be attributed to $CO_2^{\delta-}$ species generated by the adsorption of CO_2 gas which also appears in the spectra {537.1 (O 1s) and 293eV (C 1s)}.[21,33] Weak features a 532.5 eV (O 1s) and 289.9 eV (C 1s) point to the presence of a small amount of formate ($HCOO^-$)[21] probably formed by reaction of CO_2 with a minor concentration of H_2 in the background gases. Subsequent addition of 270 mTorr of H_2 and heating to 400 (d) and 500 K (e) produces an enhancement of the features for $HCOO^-$. The small feature at 284 eV, assigned to surface C on the surface (see above), remains more or less constant through the entire experiment. A similar AP-XPS experiment for plain Cu(111) exposed to a mixture of CO_2/H_2 showed only $HCOO^-$ which is produced by direct reaction of CO_2 with adsorbed H atoms.[89,] Thus, the $CO_2^{\delta-}$ appears on the surface only after the formation of the ceria-copper interface.

A comparison of the results in Figures 13 and 14 shows a correlation between the catalytic activity, the presence of Ce^{3+} sites and the generation of $CO_2^{\delta-}$ surface species.[21] This trend supports a theoretical study which suggests that Ce^{3+} sites and adsorbed $CO_2^{\delta-}$ are essential in the $CO_2 \rightarrow CH_3OH$ conversion.[33] The reaction mechanism predicted by the

theoretical calculations involves first the reverse water-gas shift reaction to generate CO and then sequential hydrogenation of this molecule: $CO \rightarrow CHO \rightarrow CH_2O \rightarrow CH_3O \rightarrow CH_3OH$.[33]

Experiments for the hydrogenation of CO_2 on $Cu/CeO_x/TiO_2(110)$ show an extremely active catalyst.[33] The Cu-CeO_x interface formed on top of the $TiO_2(110)$ substrate is quite efficient for binding and activating CO_2 producing a catalyst that is several orders of magnitude better than Cu(111) and also superior with respect to CeOx/Cu(111).[33] Synergistic interactions between the supported ceria and copper nanoparticles could be responsible for this trend.[84]

6 . Activation and dry reforming of methane

Due to the abundance of CO_2 and CH_4 in natural and land-fill gas, basic research on their conversion into useful reactants/fuels has peaked.[90] The catalytic dry reforming of methane (DRM: $CH_4 + CO_2 \rightarrow 2H_2 + 2CO$) has shown to be one promising method for this transformation producing synthesis gas that can be upgraded into liquid fuels.[90,91,] Four key challenges exist with the DRM process: 1) CH_4 conversion, 2) CO_2 activation, 3) little understanding of the mechanism for CO and H_2 production, and 4) catalyst deactivation from coke formation.[90-92] A fundamental study with a model $Ni/CeO_2(111)$ catalyst has helped to address these issues.[34]

Powders of Ni-CeO_2 are highly active, stable, and coke resistant DRM catalysts.[34] While bulk Ni may be active towards DRM, it requires high reaction temperatures and suffers from a rapid deactivation due to coke formation, which passivates the surface.[93,94,95] A strong metal support interaction (SMSI) between Ni and CeO_2 [77] leads to high activity and stability not observed on either component of the catalysts alone.[34] The low loading of Ni, firmly bound to the CeOx surface enables catalytic chemistry.[34,77] Figure 15 shows the C 1s and Ce 4d + Ni 3p photoemission spectra of the $Ni/CeO_2(111)$ catalyst under 100 mTorr of CH_4 at several temperatures.[34] The C 1s reveals CH_4 activation at 300K in the form of CH_x (285 eV) and carbon from methane full dissociation reacts with lattice oxygen to form CO_x (290

eV) without the formation of carbon deposits or nickel carbides. The Ce 4d + Ni 3p regions reveal that a significant reduction of Ce^{4+} to Ce^{3+} and Ni^{2+} to Ni^{0} occurs at 700 K in the presence of 100 mTorr CH_4. It is noteworthy that this reduction of ceria and absence of coking or carburization is not observed on the individual components.[34]

The same catalyst in the presence of both CH_4 and CO_2 yields interesting results as well. Figure 16 shows the C 1s and Ce 4d + Ni 3p regions during the simultaneous exposure to 100 mTorr CH_4 and 100 mTorr CO_2.[34] A marked increase in CO_x is observed at 300 K from the activation of CO_2 on the ceria surface. Additionally, at 700 K gas phase CO and adsorbed CO_x peaks are observed in the C 1s indicative of DRM activity. An important observation is the lack of carbide or carbon deposits in the C 1s. This also reveals the high stability of the catalyst, which is due to the ability of ceria to provide oxygen species, through the partial dissociation of carbon dioxide ($CO_2 \rightarrow CO + O$), that prevent coke formation.[34] The Ce 4d + Ni 3p regions do not change until 700 K, where catalytic activity begins and a subsequent reduction of Ni^{2+} to Ni^{0} and partial reduction of Ce^{4+} to Ce^{3+} occurs. These findings correspond well with in situ XRD results from the powdered catalyst under DRM reaction conditions, which indicate that the active phase consists of metallic Ni on partially reduced ceria.[34]

Another study elucidates the Ni coverage dependence on the enhanced activity and stability of the Ni/CeO_2(111) surface.[96] The overall conclusions from the authors are that, while low Ni coverages (< 0.2 ML) exhibit high DRM activity and stability, increasing the Ni coverage (> 0.2 ML) results in decreased activity and the carburization of Ni that ultimately leads to coking induced deactivation. Figure 17 shows the C 1s region of CeO_2(111), 0.15 ML Ni/CeO_2(111), and 0.4 ML Ni/CeO_2 after a 5 min exposure to 1 Torr methane at 300 K. The low Ni coverage results in CH_x and CO_x species from the activation of methane and interaction of C species with lattice O.[34,96] However, increasing the Ni coverage to 0.4 ML causes a bulk-like behavior of Ni resulting in decreased methane activation (lower concentration of CH_x and CO_x) along with the formation of NiC_x species. The study goes on

to demonstrate the dependence of methane activation on Ni coverage showing that further increasing the Ni coverage results in the elimination of low temperature methane activation (NiC_x is the only species present in the C 1s region at > 0.4 ML Ni). Furthermore, DRM activity peaks at 0.15 ML Ni coverage, after which it drops rapidly.[96] The research with the model Ni/CeO_2(111) systems elucidated the crucial role the SMSI effect has on DRM catalysis and how the interface between metal and support can drive reaction mechanisms.

7 . Conversion and reforming of alcohols

The chemistry of alcohols on well-defined surfaces of ceria has been the subject of a large number of studies.[28,40,97,98] Methanol, ethanol, 1-propanol, and 2-propanol react with a well-ordered CeO_2(111) thin film at low temperature forming alkoxy and hydroxyl species on the surface.[97] On fully oxidized CeO_2(111), recombination occurs between some of the alkoxys and hydroxyls, yielding alcohol desorption near 220 K. At the same temperature, some of the surface hydroxyls disproportionate to produce water and the loss of lattice O. The remaining alkoxys react above 550 K. The primary alcohols favor dehydrogenation products (aldehydes). There is a net loss of O from the system, resulting in formation of CeO_x. The secondary alcohol, 2-propanol, undergoes primarily dehydration, producing propene with no net change in the cerium oxidation state.[97] Reduced CeO_X(111) competes with the gaseous products for available O. Little or no water is produced. The reaction selectivity for the C_2 and C_3 alcohols shifts toward favoring dehydration products. These studies[40,97,98] give a useful background to study catalytic processes involving alcohols.

A. Partial oxidation of methanol.

Reaction of methanol with oxygen can lead to the selective formation of formaldehyde[28] or the production of molecular hydrogen and carbon dioxide ($CH_3OH + 1/2O_2 \rightarrow 2H_2 + CO_2$).[99] Vanadia supported on ceria shows a remarkable activity for selective oxidation reactions.[100,101] The selective oxidation of methanol to formaldehyde was studied on a well-defined VO_x/CeO_2(111) model system for which the atomic surface structure has been determined.[102] There is experimental evidence for the presence of isolated monomeric vanadia species with vanadyl goups and vanadium in the +5 oxidation state. Temperature-

programmed desorption at low vanadia loadings revealed reactivity at much lower temperature (310-430 K in Figure 18) as compared to pure ceria and vanadia on inert supports such as silica.[99] Calculations based on Density functional theory indicate that the special structural and electronic properties of VO_2 units dispersed on ceria facilitate the dehydrogenation of methanol (Figure 18).[99] At the origin of this support effect is the ability of ceria to stabilize reduced states by accommodating electrons in localized f-states.[99]

Catalysts with a CeO_x/Pt configuration exhibit high activity for the production of hydrogen through the partial oxidation of methanol.[99] Adding a non-continuous adlayer of ceria greatly enhances the catalytic performance of Pt gaining an order of magnitude in the yield of hydrogen. It has been suggested that the methanol oxidation process is facilitated by the synergistic effect between both components of the inverse catalyst (involving oxygen from ceria and providing a reaction site on the adjacent Pt surface).[99]

B. Ethanol steam reforming

Ethanol steam reforming (ESR: $C_2H_5OH + 3H_2O \rightarrow 6H_2 + 2CO_2$) is of great interest to the chemical industry for the production of hydrogen from a compound easily generated from biomass fermentation.[103,104] It is generally accepted that the reaction requires bifunctional catalysts, with the metal component contributing to the C-C/C-H bond scissions of ethanol while the oxide support helps with the dissociation of water and dehydrogenation (dehydration) of ethanol. Thus, ceria-supported metal-oxide catalysts have been well studied for this reaction due to the redox properties of ceria.[103,105,106,107] Furthermore, to understand the ethanol chemistry in a molecular level, studies have also been expanded to model catalysts under well-defined conditions with surfaces such as $CeO_2(111)$,[97] Pt-$CeO_2(111)$,[108] Co-$CeO_2(111)$[109] and Ni-$CeO_2(111)$.[35,110]

Photoemission experiments and theoretical calculations have shown that the dissociation of water, one half cycle of the ESR reaction, on Ni-$CeO_2(111)$ and Pt-$CeO_2(111)$ surfaces is a fast process.[111, 112] Figure 19 presents the interaction of water with the Pt deposited $CeO_2(111)$ surface, whereas the dissociation of water and formation of hydroxyl

groups readily takes place at temperature as low as 180 K.[112] Further increasing the surface temperature up to 500 K will lead to the fully decomposition of water, giving rise to the formation of atomic oxygen and hydrogen on the surface that are essential for the ESR reaction.

On the other hand, the interaction of ethanol with Pt deposited on CeO_2(111) surfaces was examined and compared with reaction patterns seen for other oxygenates, such as ethylene glycol and acetic acid.[108] For ethanol, deprotonation and facile formation of ethoxy species prevailed at low temperature. Pure ceria is not capable of breaking the C-C bond in ethanol. In contrast, peaks for atomically adsorbed carbon together with a small fraction of adsorbed CO were found on the Pt(111) surface at 350 K, suggesting the C-C scission of ethanol. The deposited carbon remained intact even at 700 K on the Pt(111) surface. On the other hand, no carbon formation was observed on Pt-CeO_2(111) at 700 K.[108] The authors attributed the removal of surface carbon to oxygen spillover from ceria to Pt at temperature above 500 K,[108,113] which will then reoxidize the surface carbon in the forms of CO/CO_2. This also applies to the case of ethylene glycol or acetic acid on Pt-CeO_2(111), in which surface carbon was accumulated at 350 K and then removed via oxidative self-cleaning driven by oxygen reverse-spillover from ceria at 700 K. The comparison between different alcohols and various surfaces highlights the role of ceria in the catalytic selectivity as an oxygen feedstock.

The reactions described above for the oxygenates on the Pt-Ceria system were all conducted in UHV conditions with only a half cycle of the reaction (only one reactant).[108] Most importantly, some structures and active phases of the catalysts only exist under steady state and can differ from those identified in UHV conditions, thus a recent study employed AP-XPS to investigate the active phases and surface intermediates of the Ni-CeO_2(111) surface under steady state reaction conditions. Ni has shown catalytic activity that is comparable to those of the more expensive noble metal catalysts.[114,115,116] Even though Ni-based catalysts are vulnerable to deactivation as a result of carbon deposition, recent

studies have found that carbon formation can be significantly suppressed by carefully tuning the Ni particle size.[113,117]

Figure 20a shows the C 1s spectra of Ni-CeO_2(111) surface (Θ_{Ni} < 0.15 ML) under 40 mTorr of ethanol at elevated temperature.[35] In the absence of water, surface species including ethoxy (287.2 eV and 286.0 eV) and dioxyethylene (288.2 eV) were detected at temperatures below 600 K.[35] An increase of the temperature to 600 K gave rise to a very broad peak feature (287.0 – 290.0 eV) as a result of the formation of multiple oxygenate species (-CO_x). More importantly, it was found that C-C bond scission in ethanol took place at 600 K as evidenced by the three features associated with non-oxygenated carbon: one at 284.8 eV is assigned to surface carbon (C^0), while the other two (283.4 eV and 282.0 eV) are attributed to the formation of nickel carbide species (Ni_3C/Ni_xC).[20, 25] Further increase of the temperature to 700 K led to a more prominent build-up of surface carbon (284.8 eV). On the other hand, in the case of an ethanol + water mixture, it was found that the chemistry of water and OH formation is pivotal to complete the reaction cycle, and may lead to the protection of the active sites and mitigate deactivation, as presented in Figure 20b. No surface carbon was detected at 700 K under steady state conditions, and a peak at 290.3 eV indicative of carbonate groups (-CO_3^{2-}) was observed, evidencing the incorporation of water to the surface carbon oxidation. Changes in the oxidation state of the catalyst were determined by monitoring the Ce 4d and Ni 3p regions.[35] A strong reduction of ceria and Ni was detected at 700 K. XPS depth profiling revealed that such severe reduction only existed at the top layers of the ceria film, which provides supplementary information to a study of powder Ni-CeO_2 catalysts by XRD, which is more bulk sensitive.[111,112] Thus, the experiments with AP-XPS demonstrate that a synergistic interplay between ceria and low loadings of Ni is crucial to the stability and selectivity of the Ni-CeO_2(111) catalyst, by facilitating oxygen transfer from water to ceria and the surface carbon oxidation.

8. Summary and outlook

Model ceria catalysts have shown to be excellent substrates for investigating fundamental aspects associated with the operation of technical catalysts. In the last fifteen years, many combinations of well-defined metal/ceria and ceria/metal systems have been prepared, involving different kinds of metals and ceria, but only a relatively small fraction of them have been tested as catalysts. So far most of the studies have been centered in a few reactions: CO oxidation, the hydrogenation of CO_2, and the production of hydrogen through the water-gas shift and the reforming of methane or alcohols. The progress has been impressive but more systematic work is necessary in this area because the benefits in technical applications can be substantial. Using these model systems one should be able to explore in detail possible correlations between the structural, electronic and catalytic properties of ceria-metal interfaces. *In-situ* techniques (XPS, XAS, IR, STM) can be combined to obtain fundamental information under reaction conditions. In addition, computational modeling can give an alternative view of the chemistry taken place over ceria and ceria-metal interfaces and offer inaccessible information on the atomic scale.[118,119] Advances made in the understanding of the active phases for the cleavage of C-O, C-H and C-C bonds must be expanded to the manipulation of other types of chemical bonds. Several studies with model ceria catalysts have shown the importance of strong-metal support interactions. This is an area that also needs more work since little is known about the properties in a metal and ceria that lead to strong-metal support interactions. In general, an improved understanding of the key factors controlling catalytic performance will permit a more rational approach to the design of novel catalysts containing ceria.

ACKNOWLEDGEMENTS

Many of the studies described above were done in collaboration with members of the Catalysis Group at Brookhaven National Laboratory and collaborators from the Universidad Central de Venezuela, the University of Seville, and the Institute of Catalysis-Madrid: A. Baber, S. Agnoli, L. Barrio, J. Carrasco, J. Evans, M.V. Ganduglia-Pirovano, J. Graciani, J. Hrbek, P. Lustemberg, S. Kundu, S. Luo, S. Ma, K. Mudiyanselage, J.-B. Park, P.J. Ramirez,

J.F. Sanz, D. Stacchiola, A. Vidal, I. Waluyo, F. Yang and X. Zhao. Many thanks to all of them. The work carried out at Brookhaven National Laboratory was supported by the US Department of Energy (Chemical Sciences Division, DE-SC0012704). Part of these studies was done at the National Synchrotron Light Source and at the Center for Functional Nanomaterials of BNL, which are supported by the U.S. Department of Energy.

References

[1] *Catalysis by Ceria and Related Materials*, A. Trovarelli and P. Fornasiero (Editors), Imperial College Press: London (UK), 2013.

[2] A. Trovarelli, *Catal. Reviews*, 1996, **38**, 439-520.

[3] A.N, Cormack, S. Lamphier, B. Wang, T. Gubb and K. Reed, *Proc. R. Soc. A,* 2016, **471**: 20150218

[4] R. Burch, *Phys. Chem. Chem. Phys.* 2006**, 8**, 5483.

[5] J.A. Rodriguez, P. Liu, J. Hrbek, J. Evans, and M. Pérez, *Angew. Chem. Int.* 2007, **46** 1329.

[6] D.R. Mullins, P.V. Radulovic, and S.H. Overbury, *Surf. Sci.* 1999, **429**, 186.

[7] V. Matolin, L. Sedlacek, I, Matolinova, F. Sutara, T. Skala, B. Smid, J. Libra, V. Nehasil and K.C. Prince, *J. Phys. Chem. C, 2008,* **112**, 3751.

[8] T. Staudt, Y. Lykhach, L. Hammer, M.A. Schneider, V. Matolin and J. Libuda, *Surf. Sci.* 2009, **603**, 3382.

[9] J.-L. Lu, H.-J. Gao, S. Shaikhutdinov, and H.J. Freund, *Surf. Sci.* 2006, **600**, 5004.

[10] M.A. Henderson, C.L. Perkins, M.H. Engelhard, S Thevuthasan, and C.H.F. Peden, *Surf. Sci. 2003,* **526**, 1.

[11] G. Liu , J.A. Rodriguez, Z Chang, J Hrbek, and C.H.F. Peden, *J. Phys. Chem. B,* 2004, **108**, 2931.

[12] A. Hornes, A. Hungria, P. Bera, A. Camara, M. Fernandez-Garcia, A. Martinez-Arias, L. Barrio, M. Estrella, G. Zhou, J. Fonseca, J.C. Hanson, J.A. Rodriguez, *J. Amer. Chem. Soc.* 2010, **132**, 34.

[13] L. Barrio, M. Estrella, G. Zhou, W. Wen, J.C. Hanson, A. Hungria, A. Hornes, M. Fernandez-Garcia, A. Martinez-Arias, and J.A. Rodriguez, *J. Phys. Chem. C,* 2010, **114,** 3580.

[14] T. Lunkenbein, J. Schumann, M. Behrens, R. Schlögl, and M.G. Willinger, *Angew. Chem. Int. Ed.* 2015, 54, 4544.

[15] U. Berner, K. Schierbaum, G. Jones, P. Wincott, S. Haq, and G. Thornton, *Surf. Sci.* 2000, **467**, 201.

[16] C. Castellarin-Cudia, S. Surnev, G. Schneider, R. Podlucky, M. Ramsey, and F. Netzer, *Surf. Sci.* 2004, **554**, L120.

[17] J.A. Rodriguez, S. Ma, P. Liu, J. Hrbek, J. Evans and M . Perez, *Science*, 2007, **318**, 1757.

[18] Y. Suchorski, R. Wrobel, S. Becker, H. Weiss, H. *J. Phys. Chem. C*, 2008, **112**, 20012.

[19] J.A. Rodriguez, P. Liu, J. Graciani, S.D. Senanayake, D.C. Grinter, D. Stacchiola, J. Hrbek and J. Fernandez-Sanz, *J. Phys. Chem. Lett.* 2016, **7**, 2627.

[20] G.-M. Schwab, *Adv. Catal*. 1978, **27**, 1.

[21] S.D. Senanayake, P.J. Ramirez, I. Waluyo, S. Kundu, K. Mudiyanselage, Z. Liu, Z. Liu, S. Axnanda, D.J. Stacchiola, J. Evans, and J.A. Rodriguez, *J. Phys. Chem. C*, 2016, **120**, 1778.

[22] U. Berner and K. Schierbaum, *Physical Review B,* 2002, **65***,* 235404*.*

[23] H.H. Kung, *Transition Metal Oxides: Surface Chemistry and Catalysis,* Elsevier: Amsterdam, 1989.

[24] J.A. Rodriguez and D. Stacchiola, *Phys. Chem. Chem. Phys*. 2010, **12**, 9557.

[25] T. Ramirez Reina, S. Ivanova, O.H. Laguna, M.A. Centeno, and J,A. Odriozola, *Applied Catalysis B: Environmental*, 2016, **197**, 62.

[26] A. Martínez-Arias, M. Fernández-Garía, L.N. Salamanca, R.X. Valenzuela, J.C. Conesa and J. Soria, *J. Phys. Chem. B*, 2000, **104**, 4038.

[27] H.L. Abbott , A. Uhl , M. Baron , Y. Lei, R.J. Meyer, D.J. Stacchiola , O. Bondarchuk , S. Shaikhutdinov, and H.J. Freund, *J. Catal.* 2010, **272**, 82.

[28] M.V. Ganduglia-Pirovano, C. Popa, J. Sauer, H. Abbott, A. Uhl, M. Baron, D. Stacchiola, O. Bondarchuk, Shaikhutdinov, and H.J. Freund, *J. Am. Chem. Soc.* 2010, **132**, 2345.

[29] T. Ramirez Reina, S. Ivanova, M.A. Centeno and J.A. Odriozola. *Catalysis Today*, 2015, **253**, 149.

[30] J.B. Park, J. Graciani, J. Evans, D. Stacchiola, S.D. Senanayake, L. Barrio, L., P. Liu, J.F. Sanz, J. Hrbek and J.A. Rodriguez, *J. Ame. Chem. Soc.* 2010, **132**, 356.

[31] C.M. Kalamaras, I.D. Gonzalez, R.M. Navarro, J.L.G. Fierro, and A.M. Eftsthiou, *J. Phys. Chem. C*, 2011, **115**, 11595.

[32] J.B. Park, J. Graciani, J. Evans, D. Stacchiola, S. Ma, P. Liu, A. Nambu, J.F. Sanz, J. Hrbek, and J.A. Rodriguez, *Proceedings of the Natl. Academy of Science* (PNAS), 2009, **106** , 4975.

[33] J. Graciani, K. Mudiyanselage, F. Xu, A.E. Baber, J. Evans, S.D. Senanayake, D. Stacchiola, P. Liu, J. Hrbek, J.F. Sanz and J.A. Rodriguez, *Science*, 2014, **345**, 546.

[34] Z. Liu, D. C. Grinter, P. G. Lustemberg, T. Nguyen-Phan, Y. Zhou, Si Luo, I. Waluyo, E. J. Crumlin, D.J. Stacchiola, J. Zhou, J. Carrasco, H. F. Busnengo, M.V. Ganduglia-Pirovano, S. D. Senanayake, and J. A. Rodriguez, *Angew. Chem. Int. Ed.* 2016, **55**, 7455.

[35] Z. Liu, T. Duchon, H. Wang, D. C. Grinter, I. Waluyo, J. Zhou, Q. Liu, B. Jeong, E. J. Crumlin, V. Matolın, D. J. Stacchiola, J. A. Rodriguez, and S. D. Senanayake, *Phys. Chem. Chem. Phys.* 2016, **18**, 16621.

[36] D. C. Grinter, C. L. Pang, C. A. Muryn, F. Maccherozzi, S. S. Dhesi and G. Thornton, *J. Elect. Spect. Rel. Phen.*, 2014, **195**, 13.

[37] D. C. Grinter, C. Muryn, A. Sala, C. M. Yim, C. L. Pang, T. O. Mentes, A. Locatelli and G. Thornton, *J. Phys. Chem. C*, 2016, **120**, 11037.

[38] D. C. Grinter, C. M. Yim, C. L. Pang, B. Santos, T. O. Mentes, A. Locatelli and G. Thornton, *J. Phys. Chem. C*, 2013, **117**, 16509.

[39] M. Alexandrou and R. Nix, *Surf. Sci.*, 1994, **321**, 47.

[40] D. R. Mullins, *Surf. Sci. Rep.*, 2015, **70**, 42.

[41] J. Lu, H.-J. Gao, S. Shaikhutdinov and H.-J. Freund, *Cat. Lett.*, 2007, **114**, 8.

[42] K.-D. Schierbaum, *Surf. Sci.*, 1998, **399**, 29.

[43] D. C. Grinter, R. Ithnin, C. L. Pang and G. Thornton, *J. Phys. Chem. C*, 2010, **114**, 17036.

[44] D. R. Mullins, P. M. Albrecht, T.-L. Chen, F. C. Calaza, M. D. Biegalski, H. M. Christen and S. H. Overbury, *J. Phys. Chem. C*, 2012, **116**, 19419.

[45] Y. Zhou, J. M. Perket, A.B. Crooks and J. Zhou, *J. Phys. Chem. Lett.*, 2010, **1**, 1147.

[46] P. Luches, L. Giordano, V. Grillo, G. C. Gazzadi, S. Prada, M. Campanini, G. Bertoni, C. Magen, F. Pagliuca, G. Pacchioni and S. Valeri, *Adv. Mater. Interfaces*, 2015, **2**, 1500375.

[47] J. A. Rodriguez and J. Hrbek, *Surf. Sci.*, 2010, **604**, 241.

[48] B. Kaemena, S. D. Senanayake, A. Meyer, J. T. Sadowski, J. Falta and J. I. Flege, *J. Phys. Chem. C*, 2013, **117**, 221.

[49] D. C. Grinter, S. D. Senanayake and J. I. Flege, *Appl. Cat. B*, 2016, **197**, 286.

[50] J. Höcker, T. Duchoň, K. Veltruská, V. Matolín, J. Falta, S. D. Senanayake and J. I. Flege, *J. Phys. Chem. C*, 2016, **120**, 4895.

[51] D. C. Grinter, C. Muryn, B. Santos, B.-J. Shaw, T. O. Menteş, A. Locatelli and G. Thornton, *J. Phys. Chem. C*, 2014, **118**, 19194.

[52] A. Allahgholi, J. I. Flege, S. Thieß, W. Drube and J. Falta, *Chem. Phys. Chem.*, 2015, **16**, 1083.

[53] J. Höcker, T. O. Mentes, A. Sala, A. Locatelli, T. Schmidt, J. Falta, S. D. Senanayake and J.-I. Flege, *Adv. Mater. Interfaces*, 2015, **2**, 1500314.\

[54] J.-I. Flege, B. Kaemena, A. Meyer, J. Falta, S. D. Senanayake, J. T. Sadowski, R. D.

Eithiraj and E. E. Krasovskii, *Phys Rev B*, 2013, **88**, 235428.

[55] S. D. Senanayake, J. T. Sadowski, J. Evans, S. Kundu, S. Agnoli, F. Yang, D. Stacchiola, J. I. Flege, J. Hrbek and J. A. Rodriguez, *J. Phys.Chem. Lett.* 2012, **3**, 839.

[56] P. G. Lustemberg, Y. Pan, B. J. Shaw, D. Grinter, C. Pang, G. Thornton, R. Perez, M. V. Ganduglia-Pirovano and N. Nilius, *Phys. Rev. Lett.*, 2016, **116**, 236101.

[57] J. A. Farmer and C. T. Campbell, *Science*, 2010, **329**, 933.

[58] J. Matharu, G. Cabailh, R. Lindsay, C. L. Pang, D. C. Grinter, T. Skála and G. Thornton, *Surf. Sci.*, 2011, **605**, 1062.

[59] J. A. Rodriguez, P. Liu, M. Perez, G. Liu and J. Hrbek, *J. Phys. Chem. A*, 2010, **114**, 3802.

[60] K. Ševčíková, L. Szabová, M. Kettner, P. Homola, N. Tsud, S. Fabris, V. Matolín and V. Nehasil, *J. Phys. Chem. C*, 2016, **120**, 5468.

[61] T. Skála, F. Sutara, K. C. Prince and V. Matolín, *J. Elect. Spect. Rel. Phen.*, 2009, **169**, 20.

[62] T. Skala, N. Tsud, K. C. Prince and V. Matolin, *J Phys-Condens Mat*, 2011, **23**, 215001.

[63] T. Skála, *Appl. Surf. Sci.*, 2008, **254**, 6860.

[64] L. Ovari, S. K. Calderon, Y. Lykhach, J. Libuda, A. Erdőhelyi, C. Papp, J. Kiss and H. P. Steinrück, *J. Cat.*, 2013, **307**, 132.

[65] Y. Zhou and J. Zhou, *Journal of Physical Chemistry Letters*, 2010, **1**, 609.

[66] Y. Zhou, J. M. Perket and J. Zhou, *J. Phys. Chem. C*, 2010, **114**, 11853.

[67] D.C. Grinter, J.B. Park, S. Agnoli, J. Evans, J. Hrbek , D.J. Stacchiola , S.D. Senanayake, and J.A. Rodriguez, *Surf. Sci.* 2016, **650**, 34.

[68] X. Yang, S. Kattel, S. D. Senanayake, J. A. Boscoboinik, X. Nie, J. Graciani, J. A. Rodriguez, P. Liu, D. J. Stacchiola and J. G. Chen, *J. Am. Chem. Soc*, 2015, **137**, 10104.

[69] Y. Zhou and J. Zhou, *J. Phys. Chem. Lett.* 2010, **1**, 1714.

[70] Y. Zhou and J. Zhou, *Surf. Sci.*, 2012, **606**, 749.

[71] A.K. Santra and D.W. Goodman, *Electrochimica Acta*, 2002, **47**, 2595.

[72] A. Kaftan, F. Kollhoff, T.-S. Nguyen, L. Piccolo, M. Laurin and J. Libuda, *Catal. Sci. Technol.* 2016, **6**, 818.

[73] A. Bruix, J.A. Rodriguez, P. J. Ramírez, S. D. Senanayake, J. Evans, J. B. Park, D. Stacchiola, P. Liu, J. Hrbek, and F. Illas, *J. Am. Chem. Soc.* 2012, **134**, 8968.

[74] X. Zheng, S. Wang, Sh. Wang, S. Zhang, W. Huang, and S. Wu, *Catal. Communications*, 2004, **5**, 729.

[75] P.V. Snytnikov, M.M. Popova, Y. Men, E.V. Rebrov, G. Kolb, V.Hessel, J.C. Schouten, and V.A. Sobyanin, *Applied Catal.A: General*, 2008, **350**, 53.

[76] F. Yang, J. Graciani, J. Evans, P. Liu, J. Hrbek, J.F. Sanz, and J.A. Rodriguez, *J. Am. Chem. Soc.* 2011, **133**, 3444.

[77] S.D. Senanayake, J. Evans, S. Agnoli, L. Barrio, T.L. Chen, J. Hrbek and J.A. Rodriguez, *Topics in Catalysis*, 2011, **54**, 34.

[78] D.W. Flaherty, W.Y. Yu, Z.D. Pozun, G. Henkelman and C.B. Mullins, *J. Catal.* 2011, **282,** 278.

[79] J. Nakamura , J.M. Campbell, and C.T. Campbell , *J. Chem. Soc. Faraday Trans.* 1990, **86**, 2725.

[80] A.A. Gokhale, J.A. Dumesic, and M. Mavrikakis, *J. Am. Chem. Soc. 2008*, **130,** 1402.

[81] J.A. Rodriguez, J. Graciani, J. Evans, J.B. Park, F. Yang, D. Stacchiola, S.D. Senanayake, S. Ma, M. Perez, P. Liu, J.F. Sanz and J. Hrbek, *Angew. Chem. Int. Ed.* 2009, **48**, 8047.

[82] K. Mudiyanselage, S.D. Senanayake, L. Feria, S. Kundu, A.E. Baber, J. Graciani, A.B. Vidal, S. Agnoli, J. Evans, R. Chang, S**.** Axnanda, Z. Liu, J.F. Sanz, P. Liu, J.A. Rodriguez, D.J. Stacchiola. *Angew. Chem. Int. Ed.*, 2013, **52**, 5101.

[83] J. Graciani, J.J. Plata, J. F. Sanz, P. Liu, and J.A. Rodriguez, *J. Chem. Phys.* 2010, **132**, 104703.

[84] J.J. Plata, J. Graciani, J. Evans, J. A. Rodriguez, and J. Fernández Sanz, *ACS Catalysis*, 2016, 6, 4608.

[85] R. Si, J. Tao, J. Evans, J. B. Park, L. Barrio, J. C. Hanson, Y. Zhu, J. Hrbek, and J. A. Rodriguez, *J. Phys. Chem. C*, 2012, **116**, 23547.

[86] J. A. Rodriguez, R. Si, J. Evans, W. Xu, J. C. Hanson, J.Tao, and Y. Zhu, *Catal Today*, 215, **240**, 229.

[87] S. Luo, Th.-D. Nguyen-Phan, A. C. Johnston-Peck, L. Barrio, S. Sallis, D. A. Arena, S. Kundu, W. Xu, L. F. J. Piper, E. A. Stach, D. E. Polyansky, E. Fujita, J.A. Rodriguez and S. D. Senanayake*, J. Phys. Chem. C,* 2015, **119**, 2669.

[88] *Carbon Dioxide as Chemical Feedstock*, Aresta, M. (editor), Wiley-VCH, New York, 2010.

[89] J. Yoshihara and C.T. Campbell, *J. Catal*. 1996, **161**, 776.

[90] D. Pakhare and J. Spivey, *Chemical Society Reviews*, 2014, **43**, 7813.

[91] R. Horn and R. Schlögl, *Catalysis Letters*, 2015, **145**, 23.
[92] J.-M. Lavoie, *Frontiers in Chemistry*, 2014, **2**.

[93] X. Du, D. Zhang, L. Shi, R. Gao and J. Zhang, *J. Phy. Chem. C*, 2012, **116**, 10009.

[94] B. Steinhauer, M. R. Kasireddy, J. Radnik and A. Martin, *Applied Catalysis A: General*, 2009, **366**, 333.

[95] S. A. Theofanidis, V. V. Galvita, H. Poelman and G. B. Marin, *ACS Catalysis*, 2015, **5**,

3028.

[96] P. G. Lustemberg, P. J. Ramírez, Z. Liu, R. A. Gutiérrez, D. G. Grinter, J. Carrasco, S. D. Senanayake, J. A. Rodriguez and M. V. Ganduglia-Pirovano, *ACS Catalysis*, 2016, **6**, 8184.

[97] D. R. Mullins, S. D. Senanayake and T. L. Chen, *J. Phys. Chem. C*, 2010, **114**, 17112.

[98] A. Beste and S.H. Overbury, *J. Phys. Chem. C*, 2015, **119**, 2447.

[99] A. Ostroverkh, V. Johánek, P. Kúš, R. Šedivá, and V. Matolín, *Langmuir*, 2016, **32**, 6297.

[100] I.E. Wachs, *Catal. Today,* 2005, **100**, 79.

[101] M.A. Bañares, *Catal. Today*, 1999, **51**, 319.

[102] M. Baron, H.L. Abbott, O. Bondarchuk, D. Stacchiola, A. Uhl, S. Shaikhutdinov, H.-J. Freund, C. Popa, M.V. Ganduglia-Pirovano, and J. Sauer, *Angew. Chem., Int. Ed.* 2009, **48**, 8006.

[103] L. V. Mattos, G. Jacobs, B. H. Davis and F. B. Noronha, *Chem. Rev.*, 2012, **112**, 4094.

[104] G. W. Huber, S. Iborra and A. Corma, *Chem. Rev.*, 2006, **106**, 4044.

[105] P. R. d. l. Piscina and N. Homs, *Chem. Soc. Rev.*, 2008, **37**, 2459.

[106] J. Llorca, N. s. Homs, J. Sales and P. R. r. de la Piscina, *J. Catal.*, 2002, **209**, 306.

[107] I. I. Soykal, H. Sohn, D. Singh, J. T. Miller and U. S. Ozkan, *ACS Catalysis*, 2014, **4**, 585.

[108] Y. Lykhach, A. Neitzel, K. Ševčíková, V. Johánek, N. Tsud, T. Skála, K. C. Prince, V. Matolín and J. Libuda, *ChemSusChem*, 2014, **7**, 77.

[109] L. Óvári, S. K. Calderon, Y. Lykhach, J. Libuda, A. Erdőhelyi, C. Papp, J. Kiss and H.-P. Steinrück, *J. Catal.*, 2013, **307**, 132.

[110] Z. Liu, T. Duchoň, H. Wang, E. W. Peterson, Y. Zhou, S. Luo, J. Zhou, V. Matolín, D. J. Stacchiola, J. A. Rodriguez and S. D. Senanayake, *J. Phys. Chem. C*, 2015, **119**, 18248.

[111] J. Carrasco, D. López-Durán, Z. Liu, T. Duchoň, J. Evans, S. D. Senanayake, E. J. Crumlin, V. Matolín, J. A. Rodríguez, and M. V. Ganduglia Pirovano, *Angew Chem. Int. Ed*. 2015, **54,** 3917,

[112] Y. Lykhach, V. Johánek, H. A. Aleksandro, S. M. Kozlov, M. Happel, T. Skála, P. St. Petkov, N. Tsud, G. N. Vayssilov, K. C. Prince, K. M. Neyman,V. Matolín, and J. Libuda, *J. Phys. Chem. C*, 2012, **116**, 12103.

[113] G. N. Vayssilov, Y. Lykhach, A. Migani, T. Staudt , G. P. Petrova, N. Tsud, T. Skála, A. Bruix, F. Illas, K. C. Prince, V. Matolín, K. M. Neyman and J. Libuda, *Nature Materials*, 2011, **10**, 310.

[114] Z. Gong, L. Barrio, S. Agnoli, S. D. Senanayake, J. Evans, A. Kubacka, M. Estrella, J. C. Hanson, A. Martinez-Arias, M. Fernández-Garcia and J. A. Rodriguez, *Angew. Chem. Int. Ed.*, 2010, **49**, 9680.

[115] W. Xu, Z. Liu, A. C. Johnston-Peck, S. D. Senanayake, G. Zhou, D. Stacchiola, E. A. Stach and J. A. Rodriguez, *ACS Catalysis*, 2013, **3**, 975.

[116] F. Frusteri, S. Freni, L. Spadaro, V. Chiodo, G. Bonura, S. Donato and S. Cavallaro, *Catal. Commun.*, 2004, **5**, 611.

[117] J. Carrasco, L. Barrio, P. Liu, J. A. Rodriguez and M. V. Ganduglia-Pirovano, *J. Phys. Chem. C*, 2013, **117**, 8241.

[118] J. Paier, C. Penschke, and J. Sauer, *Chem. Rev.* 2013, **113**, 3949.

[119.] A. Bruix, and K.M. Neyman, *Catal. Lett.* 2016, 146, 2053.

Figure captions.

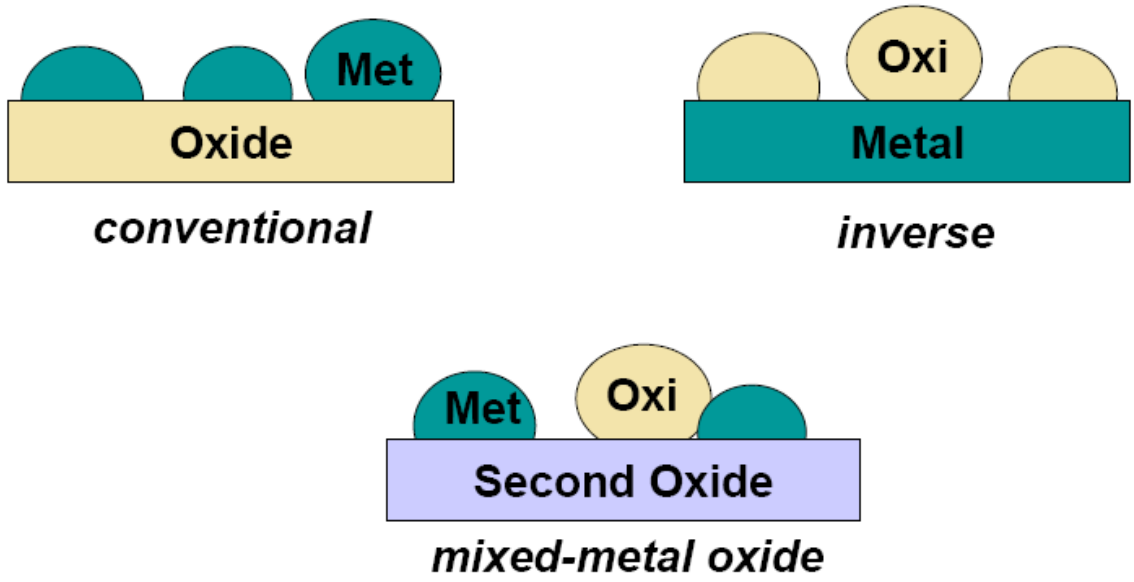

Scheme I. Different metal-oxide configurations used in studies with ceria model catalysts

(i) Deposition at high temperature (reactive deposition)

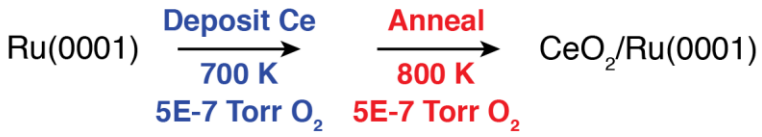

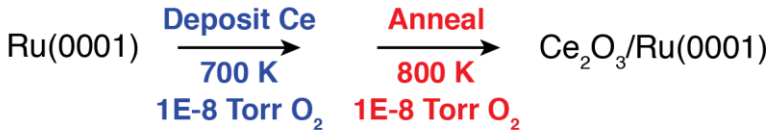

(ii) Deposition at low temperature (kinetically limited growth)

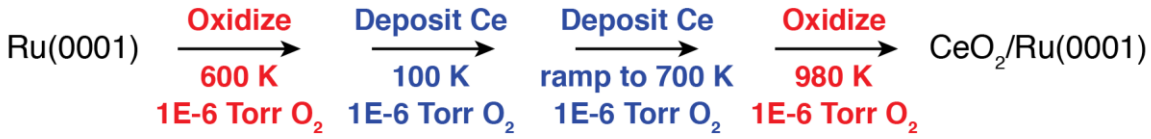

(iii) Growth via surface alloy (post-oxidation)

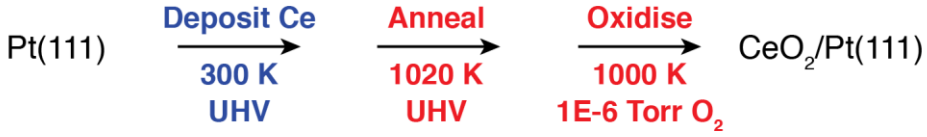

Scheme II. Comparison of the standard preparation recipes for supported CeO_2 films and nanostructures.

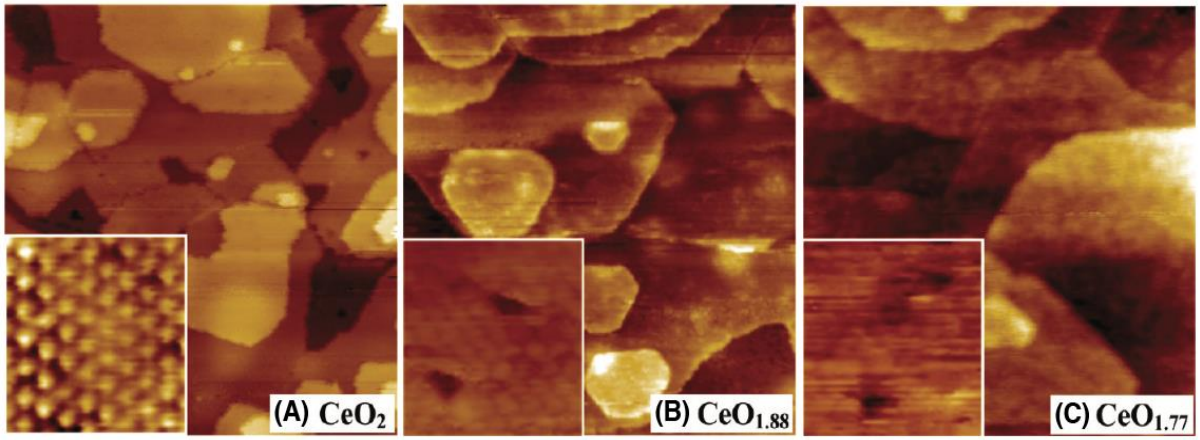

Figure 1. STM images of complete CeO_x(111) films prepared on Ru(0001), with varying ceria stoichiometry. (100 × 100 nm^2). Taken from ref. 45. Copyright 2010 American Chemical Society.

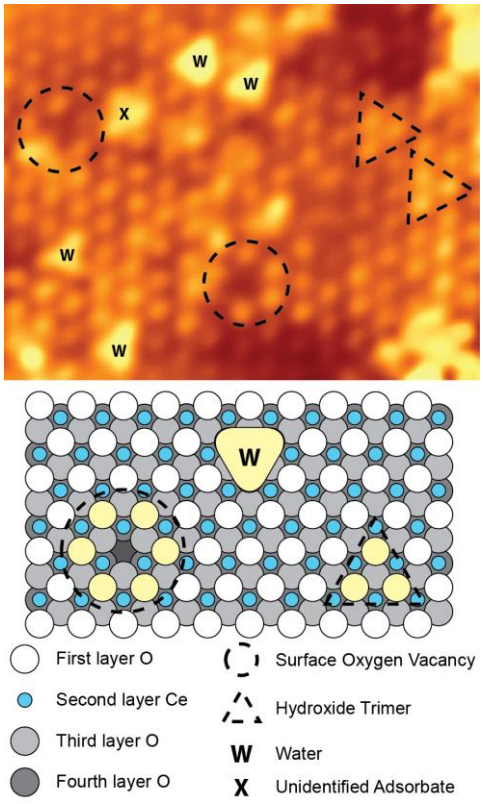

Figure 2. Atomically-resolved STM image of the CeO_2(111)/Pt(111). (7 × 6 nm^2, V = -3.0 V, I = 0.25 nA) Taken from ref. 43. Copyright 2010 American Chemical Society.

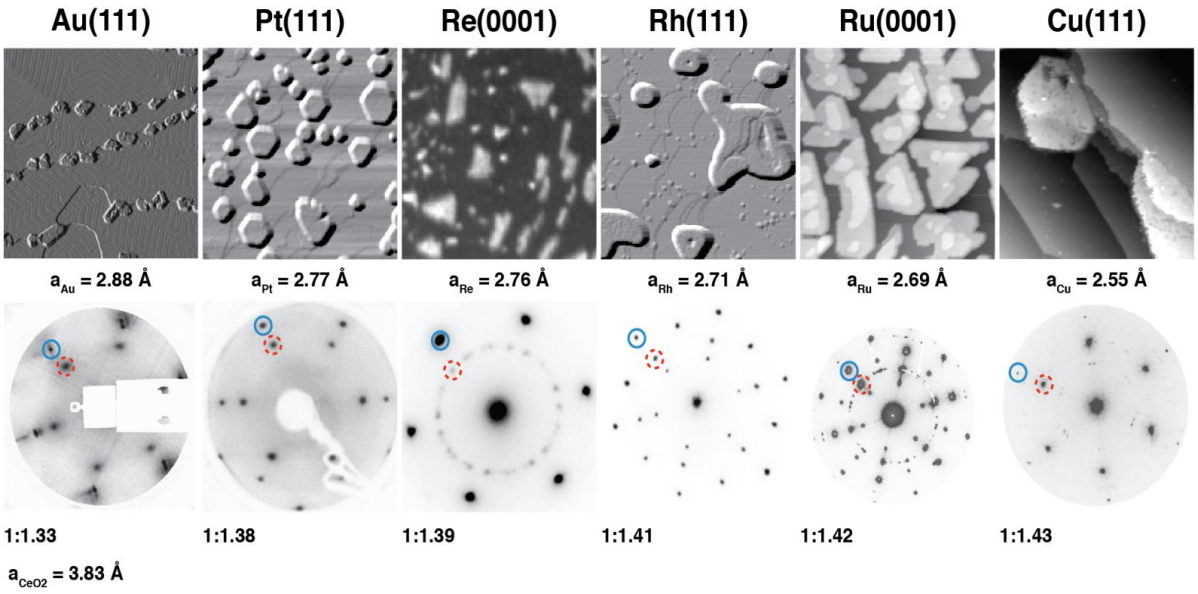

Figure 3. A comparison in real (STM, LEEM) and reciprocal space (LEED) of well-defined inverse ceria structures on a range of metals. (200 × 200 nm^2) Taken from ref. 19. Copyright 2016 American Chemical Society.

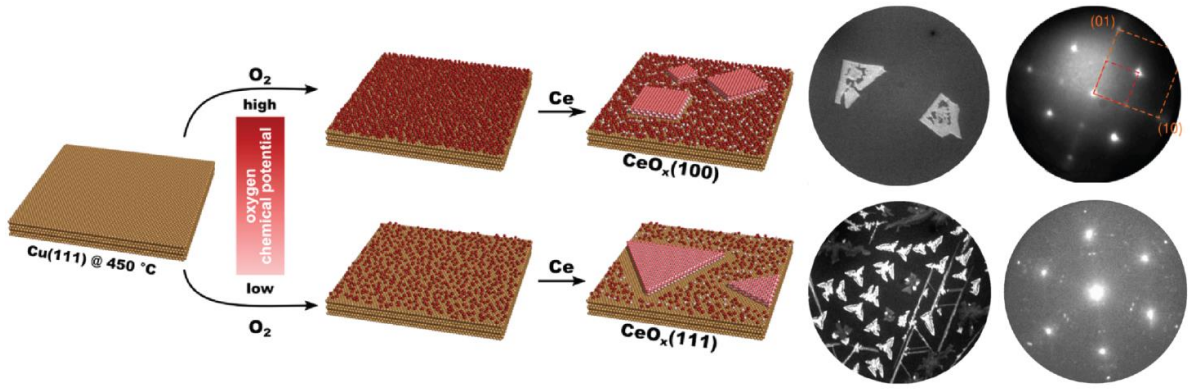

Figure 4. Preparation scheme for CeO_2 nanostructures with (100) or (111) terminations supported on Cu(111), with accompanying LEEM images and LEED patterns. (FOV = 4 μm) Taken from ref. 50. Copyright 2016 American Chemical Society.

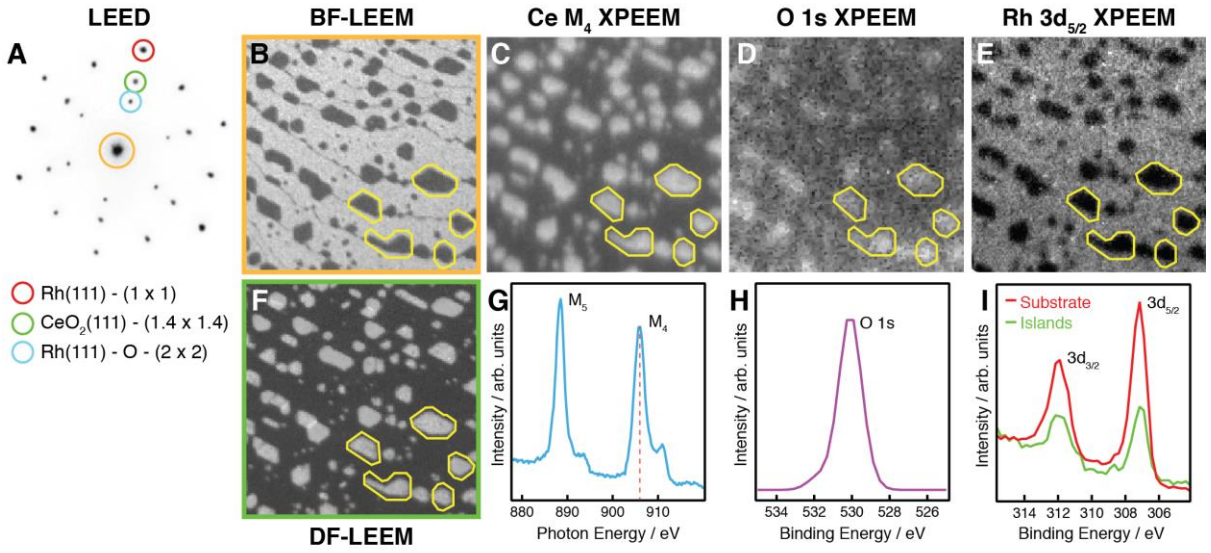

Figure 5. The characterization of a CeO_2(111)/Rh(111) inverse model catalyst with LEEM/XPEEM; the areas sampled are the same, a number of ceria islands have been highlighted in yellow. (2 × 2 μm^2) Taken from refs. 37 and 51. Copyright 2014 and 2016 American Chemical Society.

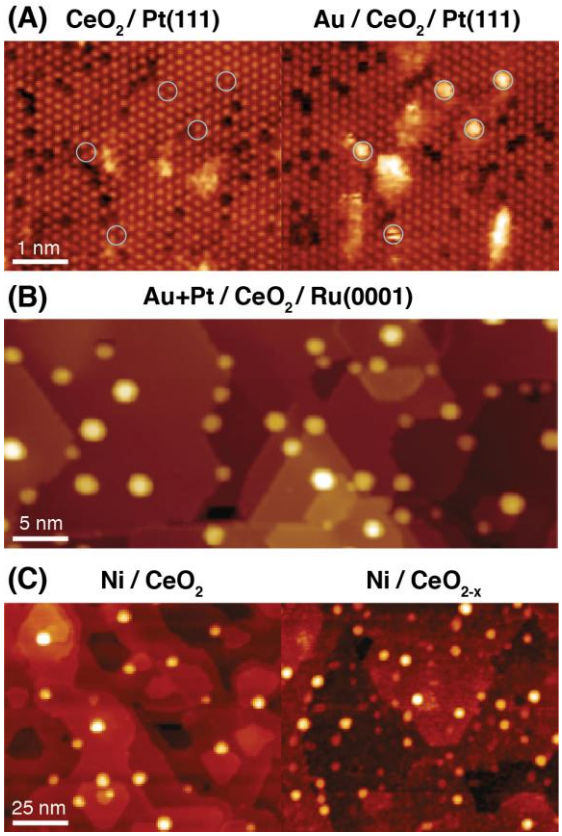

Figure 6. STM images of supported metal particles on ceria. **(A)** Au atoms supported on CeO_2/Pt(111), (10.5 × 8 nm^2) **(B)** Bimetallic Au+Pt nanoparticles on CeO_2/Ru(0001), (100 × 40 nm^2) and **(C)** Ni nanoparticles on CeO_2/Ru(0001) and CeO_{2-x}/Ru(0001). (120 × 100 nm^2) Taken from refs. 56, 65 and 66. Copyright 2016 American Physics Society and 2010 American Chemical Society.

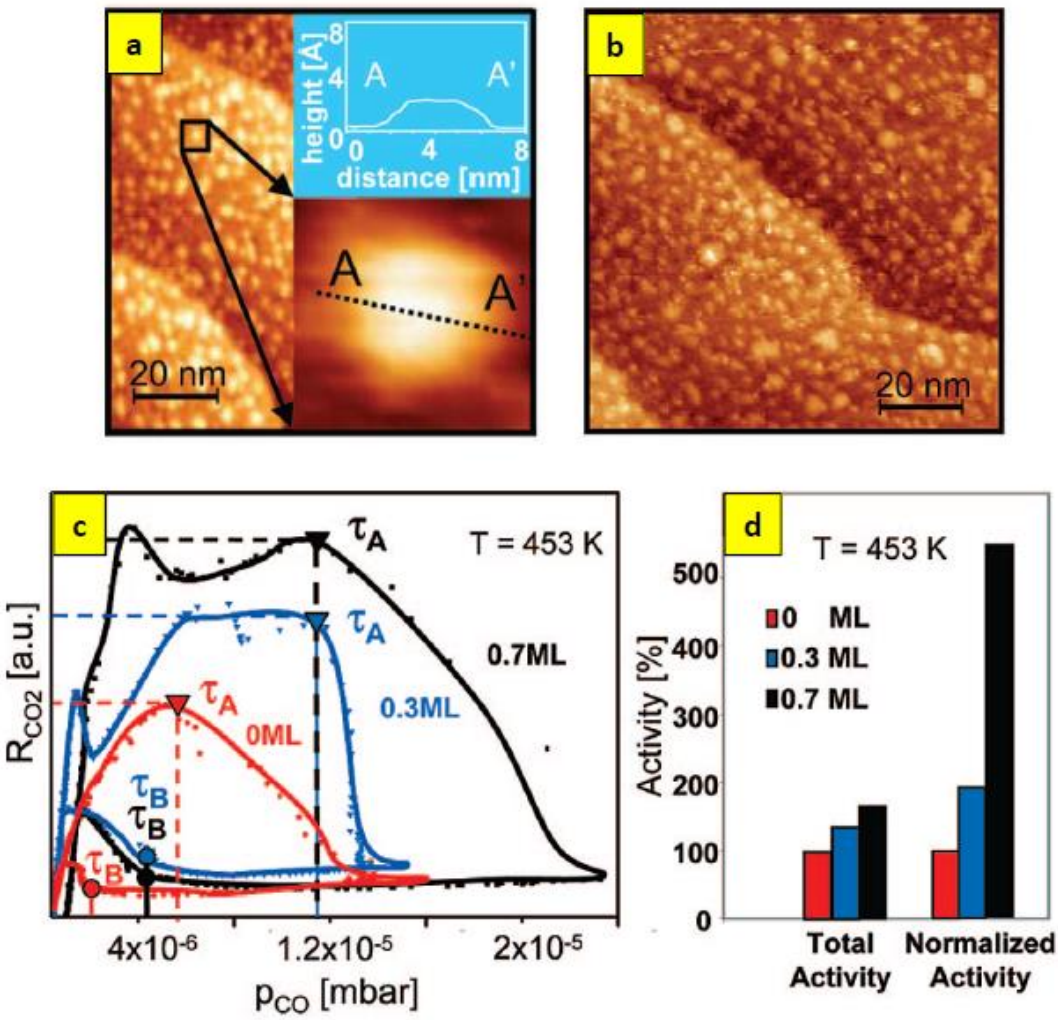

Figure 7. Top: STM images for 0.3 (a) and 0.7 (b) monolayers of CeO_x on Pt(111). Bottom: Data for CO oxidation. (c) Comparison of the hysteresis loops obtained for the clean Pt(111) surface and for the CeO*x* -0.3 ML/Pt(111) and CeO*x* -0.7ML /Pt(111) systems at *T* = 453 K and p_{O2} = 1.3 × 10-5 mbar. The maximum in the CO_2 production rate, R_{CO2}, is used as a measure of the catalytic activity of the corresponding system for comparison in (d). (d) Comparison of the catalytic activity of the clean Pt(111), CeO*x*-0.3/Pt(111) and CeO*x*-0.7/Pt(111) systems toward CO oxidation. Left side bars: total activity; right side bars: activity normalized by the exposed (bare) Pt(111) surface. Taken from ref. 18. Copyright 2008 American Chemical Society.

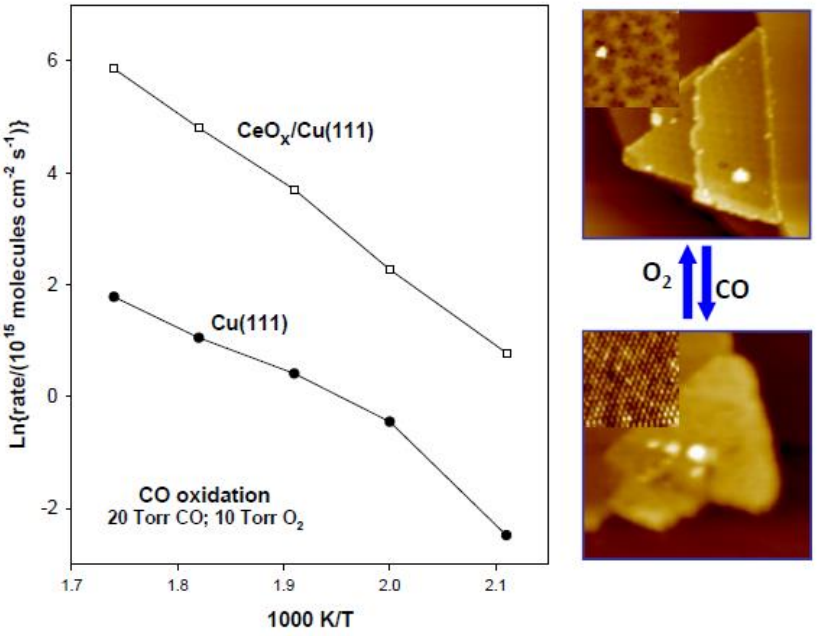

Figure 8. Left side panel: Arrhenius plots for the oxidation of CO on Cu(111) and CeOx/Cu(111) surfaces (20 Torr of CO; 10 Torr of O_2). Right side panel: STM images for the CeOx/Cu(111) surface upon reduction with CO and oxidation with O_2. Taken from ref. 76. Copyright 2011 American Chemical Society.

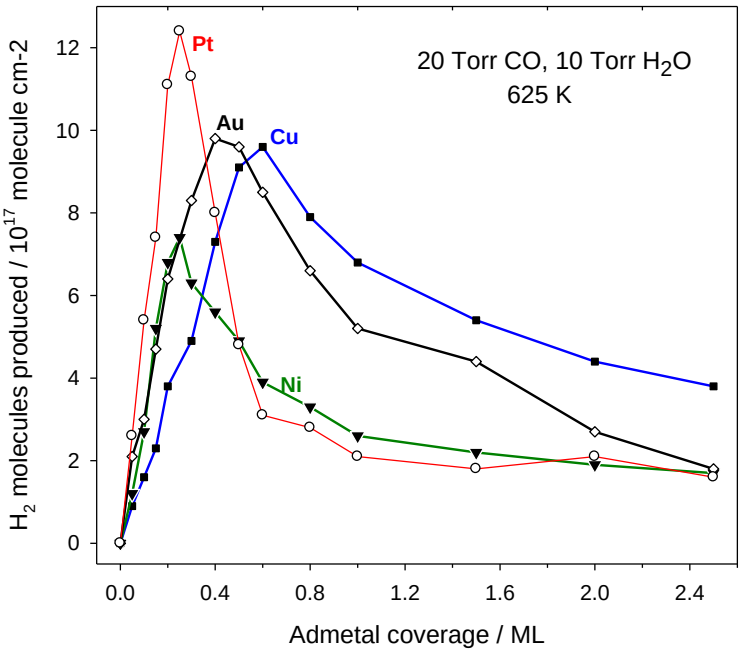

Figure 9. Production of H_2 through the water-gas shift on catalysts generated by depositing Pt, Ni, Cu and Au on CeO_2(111). T= 625 K, 20 Torr of CO, 10 Torr of H_2O for a 5 min exposure. Taken from ref. 73. Copyright 2012 American Chemical Society.

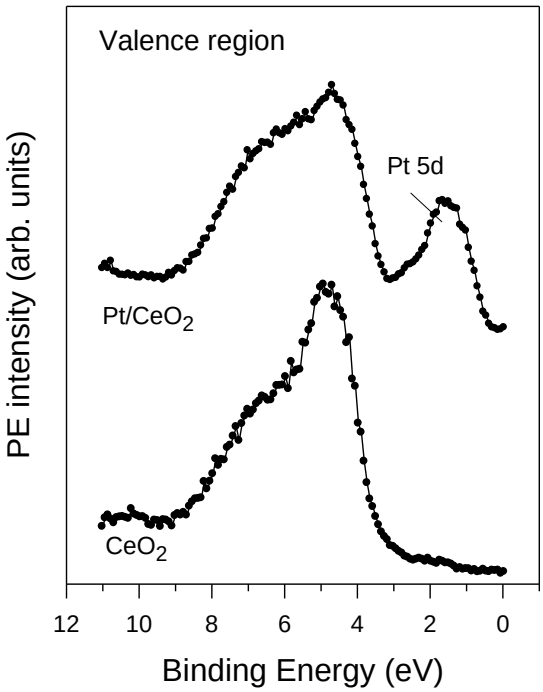

Figure 10. Valence photoemission spectra for clean CeO_2(111) and for 0.15 monolayer of Pt on CeO_2(111) surfaces. Taken from ref. 73. Copyright 2012 American Chemical Society.

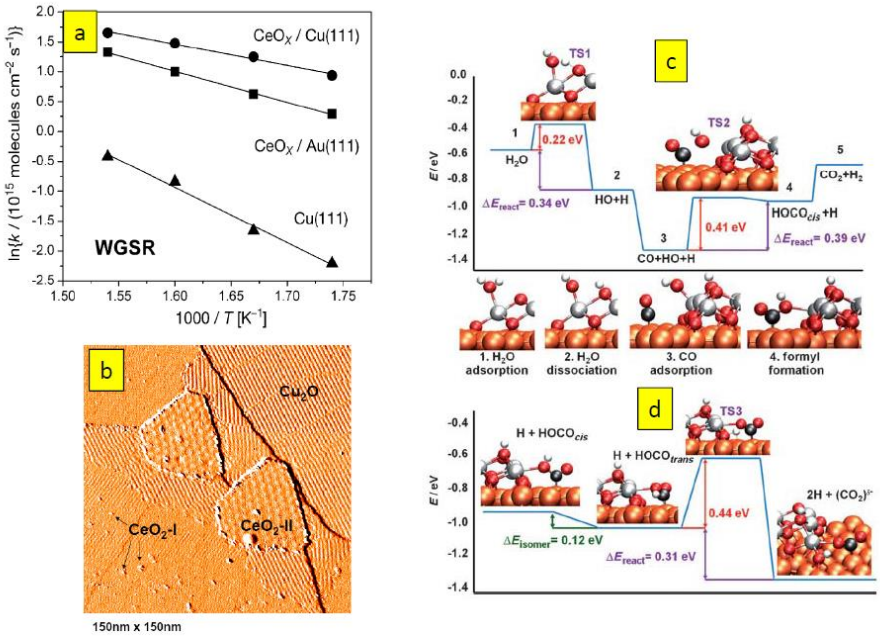

Figure 11. a) Arrhenius plots of the water-gas shift rate (CO: 20 Torr, H_2O: 10 Torr) on clean Cu(111), CeOx/Cu(111), and CeOx/Au(111). b) STM image for a CeO_x/CuO_x/Cu(111) before exporure to a CO/H_2O reaction mixture. c and d) Calculated reaction mechanism for the water-gas shift on CeO_x/Cu(111). Taken from ref. 82. Copyright 2013 Wiley.

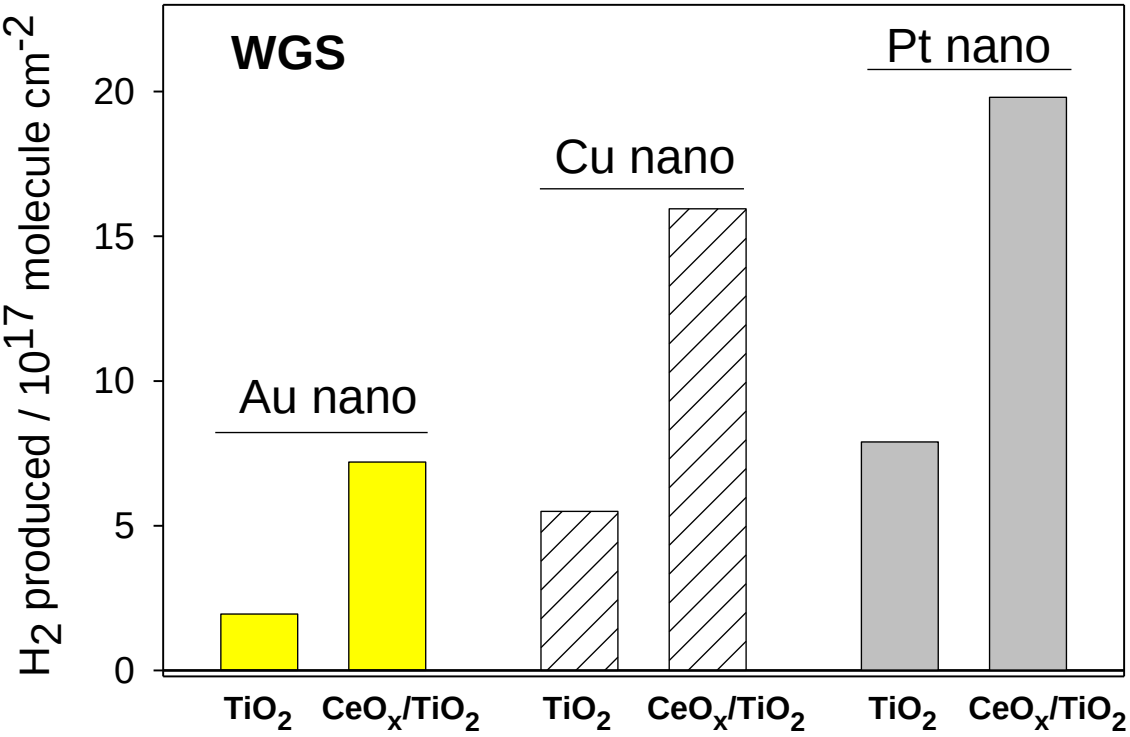

Figure 12. Production of H_2 through the water-gas shift on catalysts generated by depositing 0.15 monolayer of Au, Cu and Pt on $TiO_2(110)$ and $CeO_x/TiO_2(110)$ surfaces. For $CeO_x/TiO_2(110)$, 12-14% of the titania surface was pre-covered with ceria nanoparticles. The reported values for the production of H_2 were obtained after exposing the catalysts to 20 Torr of CO and 10 Torr of water at 625 K for 5 min. Taken from ref. 30. Copyright 2010 American Chemical Society.

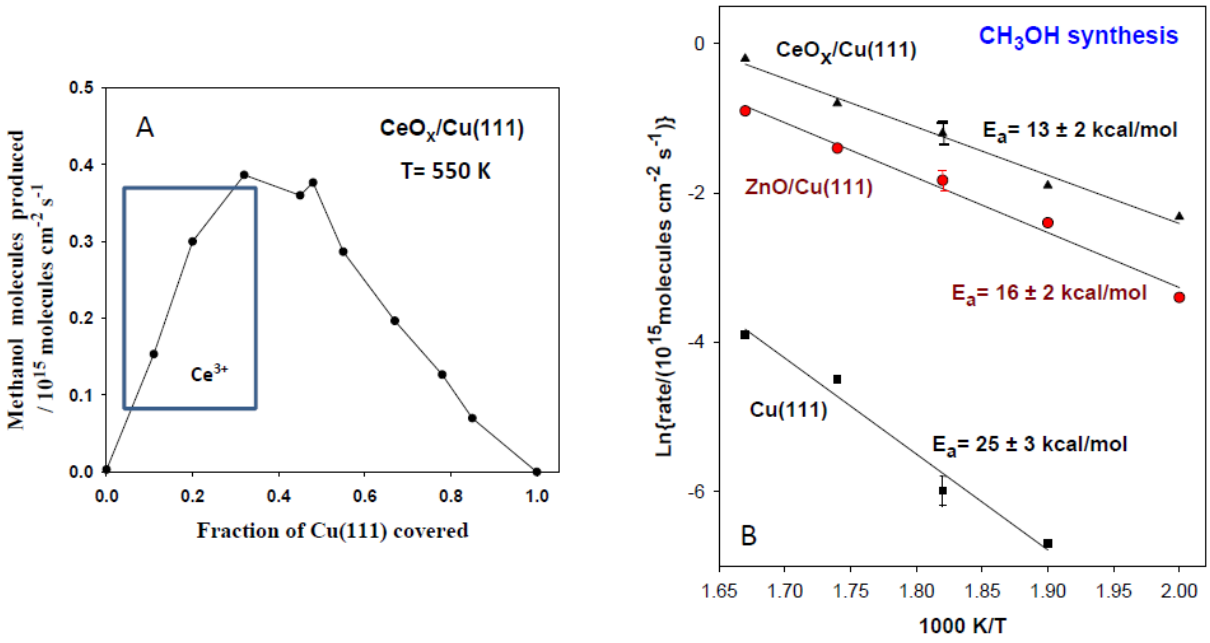

Figure 13. A) Rate for the conversion of CO_2 to methanol on Cu(111) as a function of the fraction of the metal surface covered by ceria. Reaction conditions: T= 550 K, P_{H2}= 4.5 atm, P_{CO2}= 0.5 atm. B) Arrhenius plots for the conversion of CO_2 to methanol on plain Cu(111) and on the metal surface covered 20% by nanoparticles of ZnO or Ce_2O_3. Reaction conditions: P_{H2}= 4.5 atm, P_{CO2}= 0.5 atm. Taken from ref. 21. Copyright 2016 American Chemical Society.

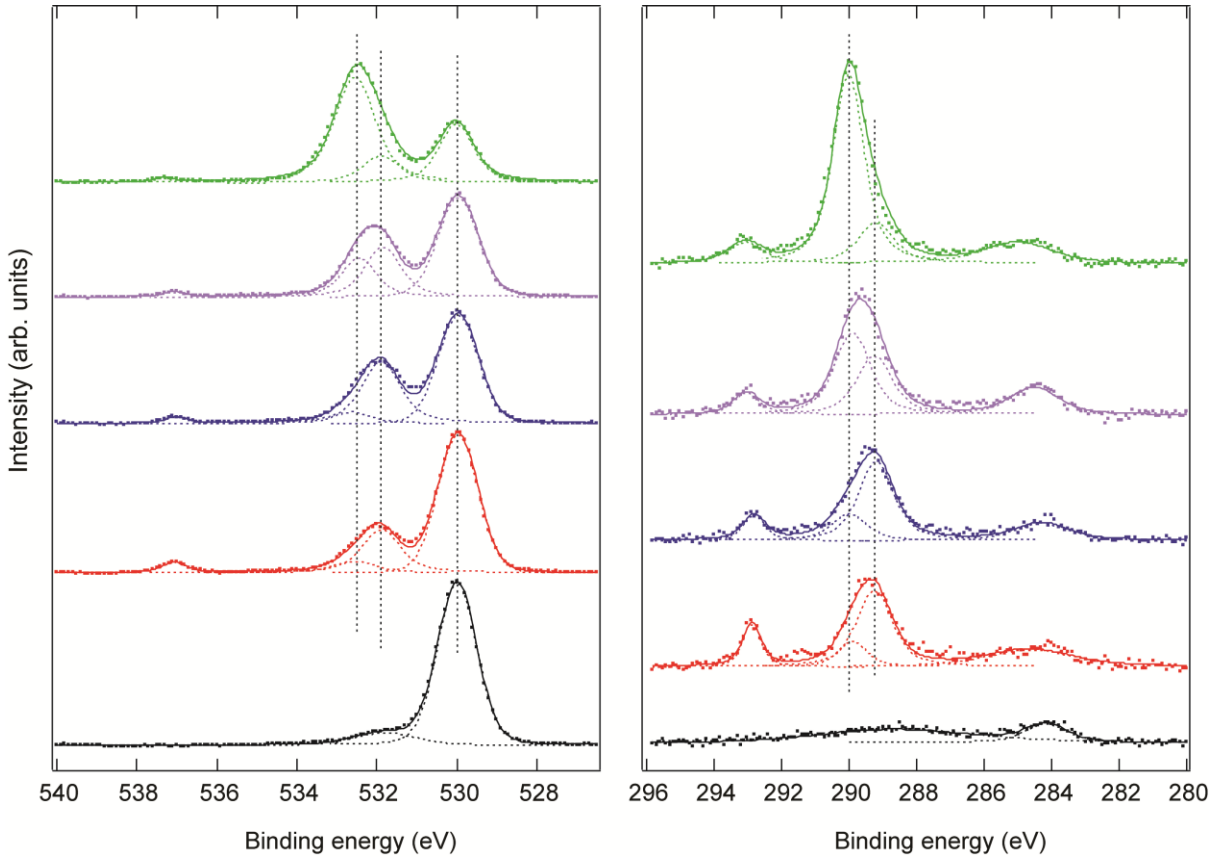

Figure 14. AP-XPS O 1s and C 1s spectra collected after exposing a CeO_x/Cu(111) surface to CO_2 and H_2 at 300, 400 and 500 K. Taken from ref. 21. Copyright 2016 American Chemical Society.

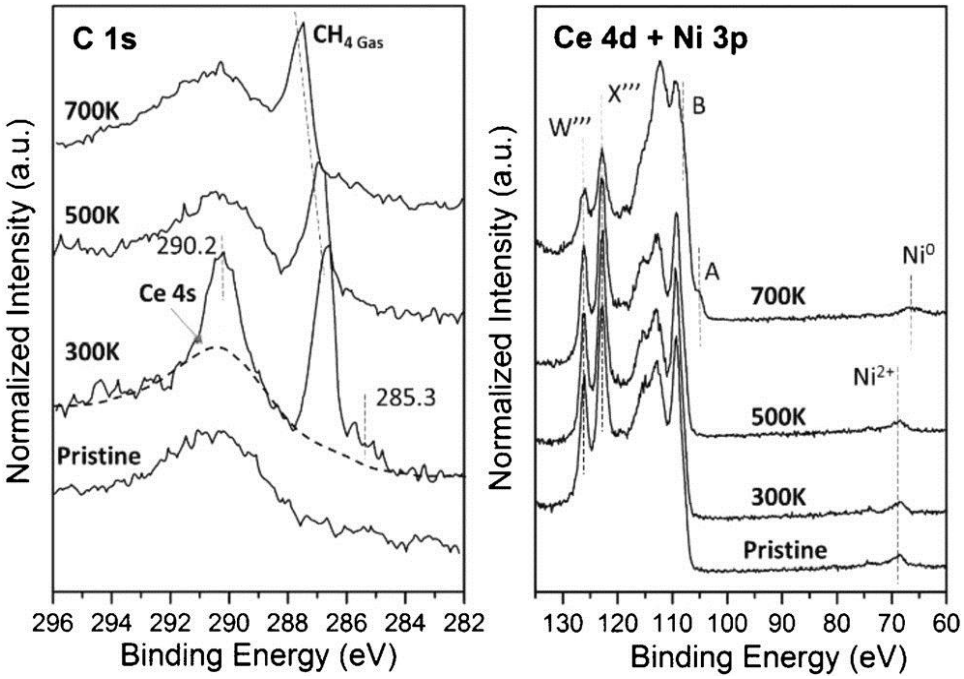

Figure 15. C 1s and Ce 4d + Ni 3p of the Ni/CeO_2(111) (θ_{Ni} = 0.1 ML) surface under 100 mTorr CH_4. Taken from ref. 34. Copyright 2016 Wiley.

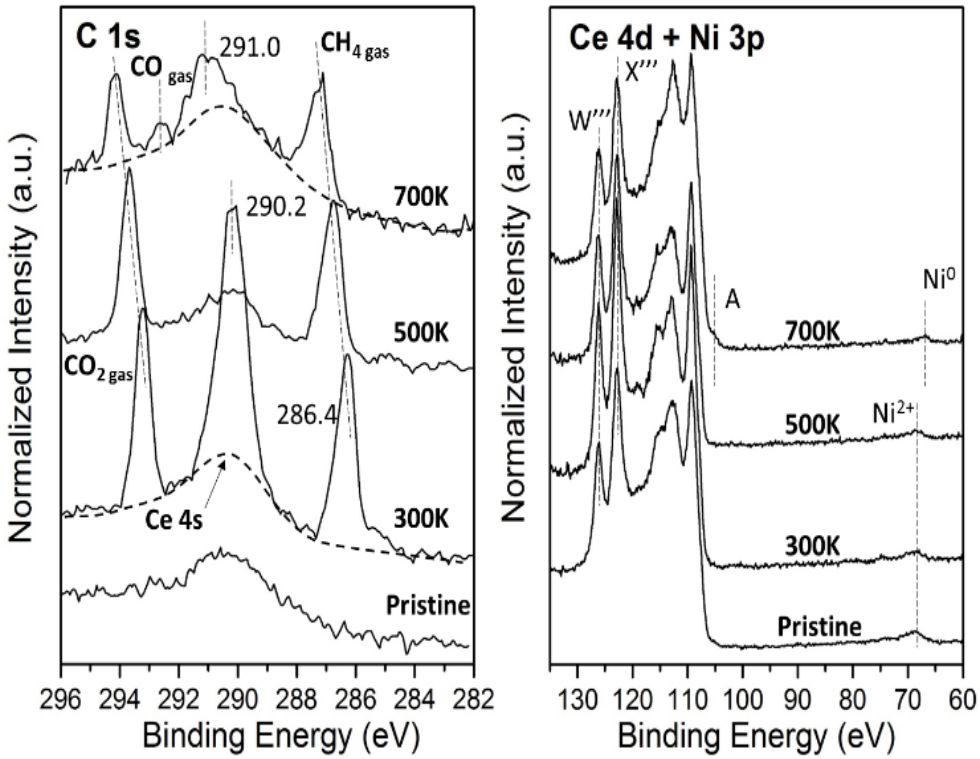

Figure 16. C 1s and Ce 4d + Ni 3p of the Ni/CeO_2(111) (θ_{Ni} = 0.1 ML) surface under 100 mTorr CH_4 + 100 mTorr CO_2. Taken from ref. 34. Copyright 2016 Wiley.

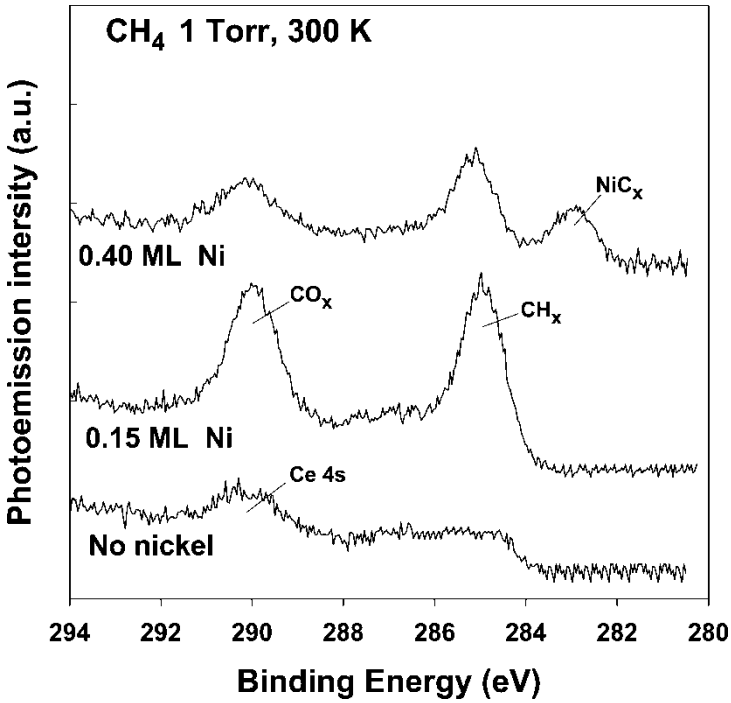

Figure 17. C 1s XPS spectra collected after exposing CeO_2(111) and Ni/CeO_2(111) surfaces to 1 Torr methane at 300 K. Taken from ref. 96. Copyright 2016 American Chemical Society.

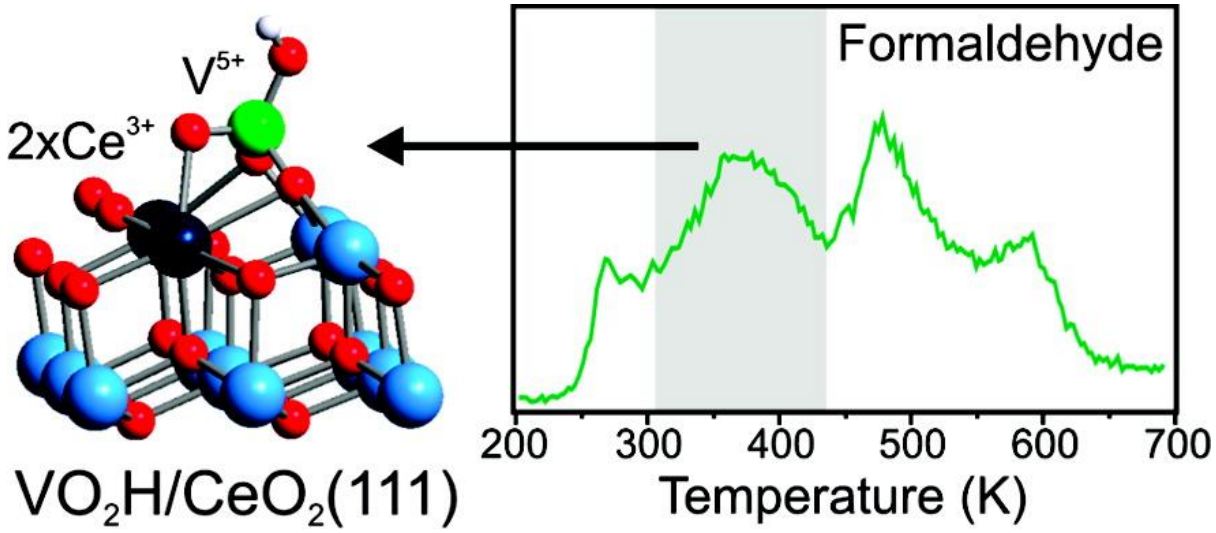

Figure 18. Left: Calculated structure for a hydrogenated VO_2 unit on CeO_2(111). Right: TPD spectra collected for the desorption of formaldehyde after dosing methanol to a VO_x/CeO_2(111) surface. Taken from ref. 28. Copyright 2010 American Chemical Society.

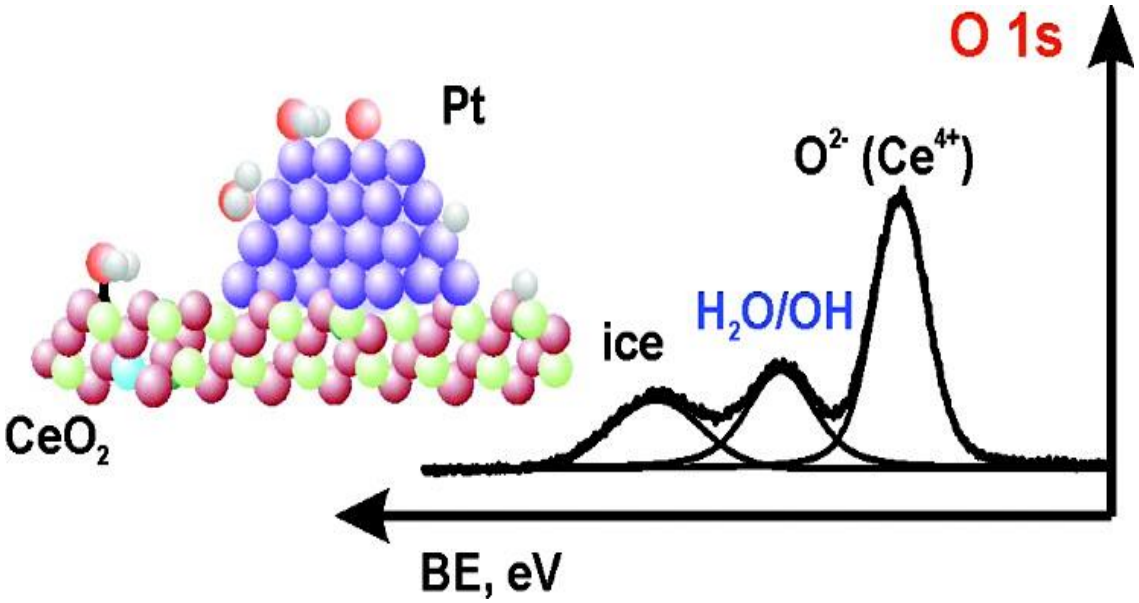

Figure 19. Left: schematic representation of water dissociation on Pt-CeO_2(111). Right: O 1s spectra of water interaction with Pt-CeO_2(111). Taken from ref. 112. Copyright 2012 American Chemical Society.

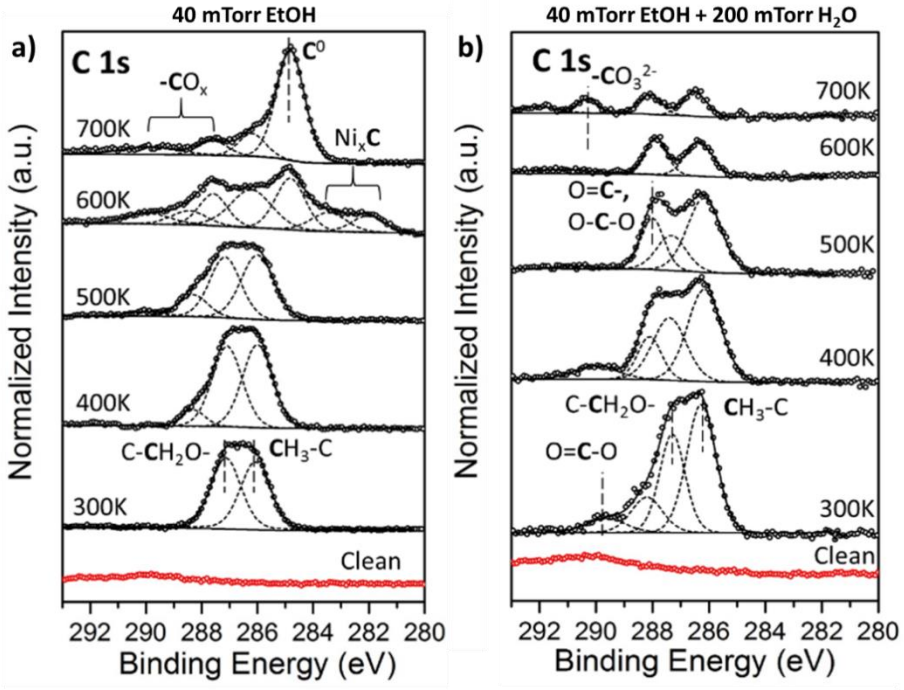

Figure 20. C 1s spectra for the Ni-CeO_2(111) surface at elevated temperature from 300-700 K: a) 40 mTorr ethanol and b) 40 mTorr ethanol + 200 mTorr water. Taken from ref. 35. Copyright 2016 Royal Society of Chemistry.